

A FINITE ELEMENT MODEL FOR PARTIALLY RESTRAINED STEEL BEAM TO COLUMN CONNECTIONS

A THESIS SUBMITTED TO
THE GRADUATE SCHOOL OF NATURAL AND APPLIED SCIENCES
OF
MIDDLE EAST TECHNICAL UNIVERSITY

BY

AHMET KÖSEOĞLU

IN PARTIAL FULFILLMENT OF THE REQUIREMENTS
FOR
THE DEGREE OF MASTER OF SCIENCE
IN
CIVIL ENGINEERING

JANUARY 2013

Approval of the thesis

A FINITE ELEMENT MODEL FOR PARTIALLY RESTRAINED STEEL BEAM TO COLUMN CONNECTIONS

submitted by **AHMET KÖSEOĞLU** in partially fulfillment of the requirements of the degree of **Master of Science in Civil Engineering Department Middle East Technical University** by,

Prof. Dr. Canan Özgen
Dean, Graduate School of **Natural and Applied Sciences**

Prof. Dr. Ahmet Cevdet Yalçiner
Head of Department, **Civil Engineering**

Assoc. Prof. Dr. Afşin Sarıtaş
Supervisor, **Civil Engineering Dept., METU**

Examining Committee Members:

Prof. Dr. Cem Topkaya
Civil Engineering Dept., METU

Assoc. Prof. Dr. Afşin Sarıtaş
Civil Engineering Dept., METU

Assist. Prof. Dr. Serdar Göktepe
Civil Engineering Dept., METU

Assist. Prof. Dr. Eray Baran
Civil Engineering Dept., Atılım University

Dr. Cenk Tort
MITENG

Date:

30/01/2013

I hereby declare that all information in this document has been obtained and presented in accordance with academic rules and ethical conduct. I also declare that, as required by these rules and conduct, I have fully cited and referenced all material and results that are not original to this work.

Name, Last Name: Ahmet Köseođlu

Signature:

ABSTRACT

A FINITE ELEMENT MODEL FOR PARTIALLY RESTRAINED STEEL BEAM TO COLUMN CONNECTIONS

Köseoğlu, Ahmet
M.Sc., Department of Civil Engineering
Supervisor: Assoc. Prof. Dr. Afşin Sarıtaş

January 2013, 53 Pages

In the analyses of steel framed structures it is customary to assume the beam to column connections as either fully rigid which means that all moments are transferred from beam to column with negligible rotation or ideally pinned that resists negligible moment. This assumption is reasonable for some types of connections. However when considering steel connections such as bolted-bolted double web angle connections it can be seen that the behavior of these connections is in between the two extreme cases. Thus a third connection type, namely semi rigid or partially restrained connection, is introduced. However this type of connection exhibits such a nonlinear behavior that modeling this behavior necessitates a substantial effort. Moreover to perform a performance based analyses the true behavior of these connections should be incorporated as part of the modeling effort. Several researches dealing with these two topics have been undertaken in literature. Despite these efforts, modeling of the moment rotation behavior of these connections still requires improvement especially under cyclic loading conditions. In addition to this, performing an analysis with existing elements incorporating semi-rigid connections as a spring attached to beam ends is not practical because of the fact that displacement based formulation increases meshing significantly which requires substantial computational power.

In this study a hysteretic (quadra-linear) moment rotation model considering pinching, damage and possibility of residual moment capacity is developed. The behavior is calibrated via experimental data available in the literature. Furthermore a force based macro element considering spread inelastic behavior along the element is presented. With this element several connections located anywhere along the beam could be incorporated in the analysis with less degree of freedom with respect to displacement based elements. Moreover the macro element model can be used in conjunction with corotational formulation for the capture of nonlinear geometric effects.

Keywords: Semi-rigid connector; nonlinear analysis; steel framed structures; finite element

ÖZ

YARI RİJİT ÇELİK KOLON KİRİŞ BAĞLANTILARI İÇİN BİR SONLU ELEMAN MODELİ

Köseoğlu, Ahmet
Yüksek Lisans, İnşaat Mühendisliği Bölümü
Tez Yöneticisi: Doç. Dr. Afşin Sarıtaş

Ocak 2013, 53 Sayfa

Çelik çerçeveli yapıların analizi genellikle kiriş kolon bağlantılarında momentlerin kirişten kolona ihmal edilebilir bir dönme ile aktarıldığı yani rijit bağlantı olduğu veya ihmal edilebilir miktarda moment taşındığı yani mafsalı bağlantı olduğu dikkate alınarak yapılır. Bu varsayım bazı bağlantı çeşitleri için makuldür. Fakat bulonlu çelik bağlantılar düşünüldüğünde bu bağlantıların davranışlarının iki uç durumun arasında olduğu görülebilir. Bu nedenle üçüncü bir bağlantı çeşidi kısmi kısıtlanmış ya da kısaca yarı rijit bağlantı tanımı ortaya çıkmıştır. Fakat bu tarz bağlantılarda meydana gelen doğrusal olmayan davranışın modellenmesi ciddi zorluklar getirmektedir. Diğer taraftan performansa dayalı bir analiz yapabilmek için bu bağlantıların gerçek davranışlarının modellenmesi gereklidir. Bu iki konuda bir çok çalışma yapılmış olmasına rağmen periyodik yüklemeler altında bu bağlantıların moment dönme davranışlarının modellenmesinde ciddi eksiklikler bulunmaktadır. Buna ek olarak yarı-rijit bağlantıların kiriş uçlarına bir yay olarak atandığı mevcut deplasman temelli kiriş elemanlarıyla analiz yapmak eleman sayısının artmasına ve ayrıca serbestlik derecelerinde artışa sebep olmaktadır ve bu da ciddi bir hesaplama gücü gerektirdiği için pratik değildir.

Bu tezde daralma (pinching) etkisi, hasar ve artık moment kapasitesinin varlığı dikkate alınarak dört doğrulu histeretik bir moment dönme modeli geliştirilmiştir. Modelin tepkisi literatürdeki mevcut deneysel veriler aracılığıyla karşılaştırılmıştır. Tezde ayrıca kiriş boyunca yayılı elastik olmayan davranışı dikkate alan kuvvet bazlı bir makro eleman modeli sunulmuştur. Bu elemanla deplasman bazlı elemanlara göre daha az serbestlik derecesi kullanarak kirişin herhangi bir yerinde olabilecek bir çok yarı rijit bağlantı analize dahil edilebilmektedir. Düğüm noktalarında oluşan deplasmanların hesabında korotasyonel (corotational) formülasyon kullanılarak doğrusal olmayan geometri etkilerinin yakalanabilmesi de mümkün olmaktadır.

Anahtar Kelimeler: Yarı-rijit bağlantı; doğrusal olmayan analiz; çelik çerçeveli yapılar; sonlu eleman

To My Family

ACKNOWLEDGEMENTS

I would like to express my sincere gratitude to my supervisor Assoc. Prof. Dr. Afşin Sarıtaş for his guidance, advice, criticism and encouragements throughout the research.

I would also like to offer my thanks to each of my family member for their patience and support during my study.

I also owe my gratitude to my roommates for providing a trustworthy and enjoyable environment.

TABLE OF CONTENTS

ABSTRACT.....	v
ÖZ.....	vi
ACKNOWLEDGEMENTS	viii
TABLE OF CONTENTS.....	ix
LIST OF FIGURES	xi
LIST OF TABLES	xiii
LIST OF SYMBOLS	xiv
CHAPTER.....	1
1 INTRODUCTION	1
1.1 Motivation of study	1
1.2 Literature Survey	2
1.2.1 Modeling of semi-rigid connections.....	2
1.2.2 Analyses of steel frames with semi-rigid connections	5
1.3 Organization of thesis.....	10
2 DEVELOPMENT OF NONLINEAR FRAME ELEMENT WITH SEMI-RIGID CONNECTORS	11
3 A HYSTERESIS SECTION MODEL FOR SEMI-RIGID CONNECTIONS	19
3.1 Presentation of hysteresis uniaxial model.....	19
3.2 Pinching	19
3.3 Existing model.....	20
3.3.1 Implementation of pinching into current model.....	23
3.4 Modified model	26
4 VERIFICATION	33
4.1 Verification of the semi-rigid mathematical model.....	33
4.2 Verification of the proposed element	39
5 SUMMARY, CONCLUSION AND RECOMMENDATIONS	43
5.1 Summary and Conclusion	43
5.2 Future research recommendations	43
REFERENCES	45
APPENDICES	47
A. STANDARDIZATION PARAMETERS AND CURVE-FITTING CONSTANT FOR FRYE-MORRIS MODEL	47
B. STUDY OF ABOLMAALI, KUKRETI AND RAZAVI	49
B.1 Connection configurations, test setup and loading history.....	49
B.2 Geometric properties of bolted-bolted and welded connections.....	51
B.3 Test results.....	52
C. PARAMETERS OF THE CURRENT MODEL.....	53

LIST OF FIGURES

FIGURES

Figure 1.1: Configuration of the geometric properties of the connections used to determine the standardization constants [6].....	3
Figure 1.2: Ultimate state configuration of connection for analytical model [7].....	4
Figure 1.3: A mechanical model example [28].....	4
Figure 1.4: A representative 3D finite element connection model, a) undeformed configuration, b) deformed configuration [14].....	5
Figure 1.5: Deformed configuration of the beam element with connections [16].	6
Figure 1.6: Effect of connection flexibility on moment distributions of beam end moments (1) single web angle; (2) double web angle, (3) top and seat; (4) end plates; (5) rigid [16].....	6
Figure 1.7: Beam model including eccentric connections [17]	6
Figure 1.8: Effect of connection flexibility on the critical load [17]	7
Figure 1.9: The beam model in which connections are modeled using a rotational spring and a dashpot [18].....	7
Figure 1.10: The adopted independent hardening model [18].....	8
Figure 1.11: Details of beam with connectors [21]	9
Figure 1.12: Ramberg–Osgood model [22]	9
Figure 2.1: Basic Forces and Deformation for Beam Element.....	12
Figure 2.2: Transformation of Element Displacements to Deformations	15
Figure 3.1: Pinching in the different behavior of different material a) shear force–deflection relation of a concrete member [30]; b) moment-rotation relation of steel connection [3]	20
Figure 3.2: Backbone curve of used tri-linear model	21
Figure 3.3: Configuration of initial, tangent and unloading stiffness values of connections [16].....	22
Figure 3.4: Positive loading and un-loading of the model	22
Figure 3.5: Positive re-loading of the model	23
Figure 3.6: Configuration of pinching behavior of the model	24
Figure 3.7: Configuration of negative energy loop.....	25
Figure 3.8: Effect of pnchy parameter with constant pnchx.....	26
Figure 3.9: Effects of pnchx and pnchy parameter on the behavior	26
Figure 3.10: Deformed shape of the bolt holes [25]	27
Figure 3.11: Experimental residual moment behavior [3]	28
Figure 3.12: Residual moment behavior of the modified model	28
Figure 3.13: Experimental example of decreasing residual moment [3]	29
Figure 3.14: Decreasing residual moment behavior of the modified model	30

Figure 3.15: Experimental example of negative residual moment [3].....	30
Figure 3.16 : A plot output of our modified model	31
Figure 4.1: DW-BB-102-16-19-114-4-406	34
Figure 4.2: DW-BB-102-10-19-114-5-533	34
Figure 4.3: DW-BB-127-13-16-114-5-610	35
Figure 4.4: DW-BB-102-13-19-114-4-610	35
Figure 4.5: DW-BB-127-10-16-114-6-610	36
Figure 4.6: DW-WB-76-13-19-89-4-610	37
Figure 4.7: DW-WB-102-16-19-89-5-610	37
Figure 4.8: DW-WB-102-10-19-89-4-610	38
Figure 4.9: DW-WB-127-13-16-114-6-610	38
Figure 4.10: DW-WB-152-19-19-191-5-610	39
Figure 4.11: The 3 storey 1 bay structure model including semi-rigid connections	40
Figure 4.12: Bilinear model for selected connection, DW-WB-152-19-19-191-5-610	41
Figure 4.13: Effects of semi-rigid connection, pinching and nonlinear geometry on story drift	42
Figure B.1: Configuration of double web angle connections: (a) bolted-bolted; (b) welded-bolted....	49
Figure B.2: Test setup and used instruments.....	50
Figure B.3: Loading history.....	50

LIST OF TABLES

TABLES

Table 1.1: The natural frequencies of the structure with varying type of connection [18]	8
Table A.1: Standardization parameters and curve-fitting constants for Frye and Morris power model (all size are in centimeters)	47
Table B.1: Geometric properties of the selected bolted-bolted connection	51
Table B.2: Geometric properties of the selected welded-bolted connections	51
Table B.3: Test results and failure modes for selected welded-bolted connections	52
Table C.1: Parameters used in the current model (All moments are in kN.m and all rotations are in radian)	53

LIST OF SYMBOLS

A: Cross sectional area of the beam element
a: Transformation matrix of local to basic deformation
b(x): Force-interpolation function
C1,C2,C3: Curve-fitting constants
 δ : Axial deformation of the connector
d1,d2,d3,d4: Respective depths of the Top and Seat Angle with Double web Angles Connection
 Δe : Section deformation increment
 Δq : Element end forces increment
drot: Rotation increment in the section model
 Δ_{sc} : Semi-rigid connection deformation vector
 ΔU : Deformation increment
DW-BB: Bolted-bolted Double Web Angle
DW-WB: Welded-bolted Double Web Angle
E: Modulus of elasticity
e(x): Section deformations of the beam element
E1p,E2p,E3p,E1n,E2n,E3n: Positive and negative slopes of the tri-linear section model
 ε_a : Axial strain of the beam element
f: Total flexibility of the beam element with connector
 f_{con} : Flexibility of the connector
 f_{elem} : Flexibility of the beam element
 $f_s(x)$: Section flexibility of the beam element
g1,g3: The Defined distances for the Top and Seat Angle with Double web Angles Connection
I: Moment of inertia
 I_a : Moment of inertia of web angle
 I_t : Moment of inertia of top angle
K: Stiffness matrix of the beam element
 κ : Curvature of the beam section
k: Stiffness of the
 $k_s(x)$: Stiffness of the beam section
Ktp,Ktn: Decreasing positive and negative residual moment slope
L: Length of the beam
M: Moment
M(x): Moment along the beam
maxmom,minmom: Positive and negative moment values at maximum and minimum rotation values respectively
momnt: Moment variable of the section model
momntP: Previous moment value in the section model
momrestp,momrestn: Positive and negative residual moments of the section model
momrestpp,momrestnn: Decreasing positive and negative residual moments of the section model
Mos: The Plastic Moment in the SeatAngle

M_{pt}: The Plastic Moment in the Top Angle
M_u: The Ultimate Moment Capacity of the Connection
N(x): Axial force along the beam
n_{IP}: Number of integration points
n_{SC}: Number of semi-rigid connectors
P_{app}: Applied forces
P_r(U): Resisting forces
θ: Rotation
q₁, q₂, q₃: Basic element forces
θ_{sc}: Rotation of semi-rigid connection
R_{ki}: Initial stiffness of the connection
R_{kt}: Tangent stiffness of the connection
rot: Current rotation value of the section model
rotch: Rotation value at the pinching point in the section model
rotlim: Limiting rotation value in the section model
rotmax, rotmin: Maximum and minimum rotation values in the section model respectively
rotpmod, rotnumod: Rotation values at the starting point of pinching during positive and negative re-loading
rotP: Previous rotation value in the section model
rotpu, rotnu: Rotation values at the starting point of positive and negative re-loading in the section model
s(x): Section forces in the beam element
s_p(x): Particular section forces in the beam element
Stiff: Stiffness at the current rotation in the section model
t_t: Thickness of the Top Angle
t_a: Thickness of the Web Angles
u₁, u₂, u₃, u₄, u₅, u₆: Global element deformations
ū₁, ū₂, ū₃, ū₄, ū₅, ū₆: Local element deformations
v₁, v₂, v₃: Basic element deformations
Vcon: Connection deformation
Vpa: The Resultant of Plastic Shear Force in a Single Web Angle
Vpt: The Plastic Shear Force in the Vertical Leg of the Top Angle
w_{IP}: Weight of integration point
w_x, w_y: Axial and transverse distributed load over the beam

CHAPTER 1

INTRODUCTION

1.1 Motivation of study

Connections constitute one of the most important parts of a structure despite the fact that they occupy a very small place in it. A structure should be well designed such that it satisfies strength, stiffness and ductility requirements, and during a strong ground shaking it should be able to dissipate significant amount of seismic energy through yielding of its members. For this purpose, moment resisting frame systems should be designed according to the strong column – weak beam design concept; thus beam ends will suffer significant reversal of bending moments during lateral movements, and the connections between the beams and columns should not be the weakest link in response. Beam to column connections of steel structures were at first made of rivets and welds. Although such connections have high moment capacity, their behavior is brittle and thus they cannot absorb seismic energy well. Furthermore, their usage in site is not practical and requires quality control and skilled labor. Fortunately, another connection type, namely bolt connection, has been considered and gained significant use in practice. The usage of these bolts is not only practical but also does not require so skilled labor, and they can be designed as rigid (moment transferring) or simple (shear transferring). But later, it has been understood that the connections assumed to be rigid or simple can undergo some rotations and carry some moments, respectively. This means that behavior of these connections is in reality semi-rigid with flexibility and significant nonlinearity incorporated in it.

American Institute of Steel Construction (AISC) classifies the connections as simple, rigid or semi-rigid according to their strength, stiffness and ductility. The use of simple connections in steel structures in seismic areas definitely necessitates the use of a lateral load resisting frame system. On the other hand, the use of rigid connections allows for the design of a structure to be a moment resisting frame type system. Rigid connections in general could suffer from brittle behavior once the moment capacity of the connection is reached as observed in Northridge Earthquake in 1994. With regards to the energy absorption, ductility and economy, the use of semi-rigid connections offers a good performance especially in seismic areas. In the last two decades, the necessity to use semi-rigid connections in steel structure is well understood by almost every designer and lots of academic research has been done in that respect. Despite this fact, the level of usage of semi-rigid connections is under the expected value due to insufficient data with regards to the cyclic behavior of these connections. Lack of experimental data is mostly due to the high cost and difficulty of conducting cyclic tests on various semi-rigid connections. For that purpose, it could be possible to conduct numerical simulations, but this also requires detailed and accurate modeling of the complex interaction of nonlinearities in the connection region and the necessity of having significant computation power to apply several cyclic loading histories.

Despite all these problems, several experimental and analytical modeling of semi-rigid connections have been performed by researchers, and implementation of an accurate behavior of semi-rigid connections into structural analyses is still a hot research issue. Furthermore, performance-based earthquake engineering necessitates the modeling of a true nonlinear behavior of buildings under

arbitrary loading and boundary conditions, and the development of modeling tools in that direction is needed. For this purpose, development of a macro element model based on force formulation and considering spread inelastic behavior along element length and incorporating nonlinear semi-rigid connectors is pursued in this thesis. With this element, nonlinear semi-rigid behavior of a column to beam connection or a column-tree to beam connection will be easily handled in an analysis. Actually, the developed element is formulated and coded such that it can include infinite number of semi-rigid connectors at arbitrary locations along an element. For a true representation of the hysteretic energy dissipation characteristic of a semi-rigid connector, a quadra-linear moment-rotation based model is developed incorporating pinching, damage, the possibility of residual moment capacity, degradation of stiffness under various scenarios. The developed moment-rotation model is calibrated and tested via experimental cyclic data of top and seat angle with/without double web angles connections from literature. The macro element model is used in conjunction with corotational formulation for the capture of nonlinear geometric effects. Analyses of steel framed structures with varying beam spans clearly demonstrate the influence of nonlinear modeling of semi-rigid connectors. An accurate capture of possible nonlinear plastification in the beam and nonlinear hinging in the connector should be strictly incorporated in the analysis of steel framed structures.

1.2 Literature Survey

In order to study the behavior of semi-rigid connections on framed structural analysis finite element programs, moment-rotation type connection models that are accurate in representing the cyclic behavior of semi-rigid connections should be available and then such a model should be implemented as part of a structural analysis program. In both aspects, several studies have been conducted, and the literature survey is thus divided into first the modeling of the semi-rigid connections and then analyses of steel framed structures with semi-rigid connection models.

1.2.1 Modeling of semi-rigid connections

Parameters that are necessary for the description of the monotonic response of a semi-rigid connection through moment-rotation type empirical model are as follows: initial stiffness, yield moment, ultimate moment and rotation. Cyclic modeling of a semi-rigid connection furthermore requires several additional parameters that are actually hard to calibrate, and very little research is available with regards to the determination of the energy dissipation characteristics of semi-rigid connections in this regards. Studies conducted on the determination of some of these parameters can be classified under the following categories: experimental, empirical, analytical, mechanical, numerical and informational[1].

1.2.1.1 Physical testing of semi-rigid connections

The most accurate way to get information about semi-rigid connection behavior is through physical testing. Conducting experiments in the laboratory could be costly and not practical especially if the tests should cover all connection types with different geometrical properties of connecting members, the use of different number of bolts, and the variations in the friction and pretension values present in the bolts. Despite these difficulties, researchers pursue such studies in order to establish a databank of the behavior of these connections for practice and for future research efforts; to name some of these: Wilson and Moore[26], Batho and Rowan[27], Popov and Takhirov[2], Abolmaali, Kukreti and Razavi [3].

Abolmaali, Kukreti and Razavi [3] tested the cyclic behavior of twenty specimens with double web angle connections with bolted-bolted and welded-bolted angles. They used both load control (at the beginning cycles) and displacement control (prior to yielding of the connections) loading protocols to apply cyclic loading on the test setup. In their paper, they presented both hysteresis moment rotation curves and failure modes of the specimens, and also compared some important properties

of the connections such as strength, ductility and stiffness with those of other connections in literature. The current study in this thesis selected the cyclic test data by Abolmaali, Kukreti and Razavi [3] in order to verify the response of the hysteretic moment-rotation type connection model, where the test setup and the comparison of the responses are also presented.

1.2.1.2 Empirical modeling of semi-rigid connections

It is obvious that the geometric and mechanical properties of the connections play an important role in the behavior of the connections. So these properties can be related with the parameters of the moment rotation behavior by performing curve fitting to experimental data [4, 5].

In the study of Frye and Morris[4], they used the power model shown in Eqn 1.1 .In this equation C1, C2 and C3 are the curve fitting constants and K is a standardization parameter which changes with the connection types (See Appendix A). It can be noted that the tangent stiffness, derivative of the moment with respect to rotation, may take negative values in some cases according to this model and this is not realistic under monotonic loading.

$$\theta = C1 * (K * M) + C2 * (K * M)^3 + C3 * (K * M)^5 \quad 1.1$$

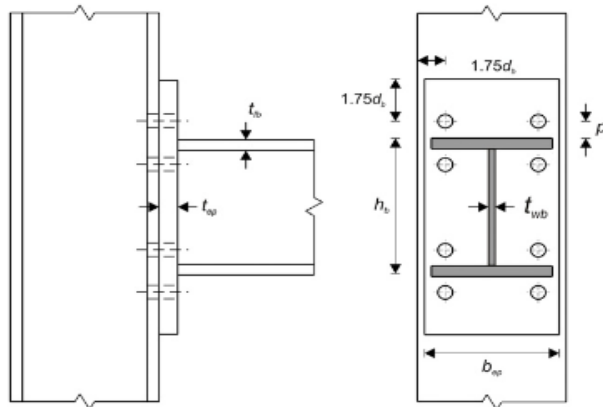


Figure 1.1: Configuration of the geometric properties of the connections used to determine the standardization constants [6]

1.2.1.3 Analytical modeling of semi-rigid connections

Analytic models[7, 8] relate the geometrical and mechanical properties of the connections using some compatibility equations and theory instead of curve fitting. Such studies utilized parameters such as ultimate and yield moment capacity of the connections by applying basic compatibility equations by means of considering ultimate or yield state configuration of the connections.

In Figure 1.2 the ultimate state configuration of the connections obtained by Kishi and Chen[7] is shown. In their study they ended up with ultimate moment capacity shown in Eqn 1.2 and initial stiffness was calculated as shown in Eqn 1.3.

$$M_u = M_{os} + M_{pt} + V_{pt}d_2 + 2V_{pa}d_4 \quad 1.2$$

$$R_{ki} = \frac{3EI_t d_1^2}{g_1(g_1^2 + 0.78t_1^2)} + \frac{6EI_a d_3^2}{g_3(g_3^2 + 0.78t_a^2)} \quad 1.3$$

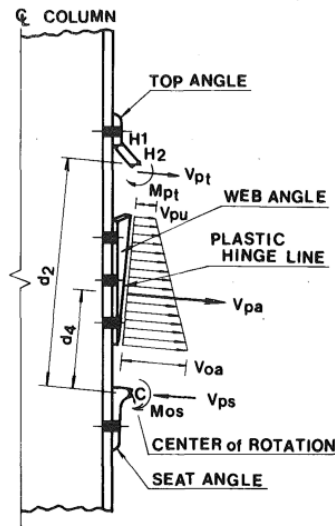


Figure 1.2: Ultimate state configuration of connection for analytical model [7]

1.2.1.4 Mechanical modeling of the semi-rigid connections

In mechanical models the connections are treated as to be composed of rigid and flexible elements. The stiffness of the related elastic elements or springs is determined by using empirical formulas. In Figure 1.3 a mechanical model example is shown [28].

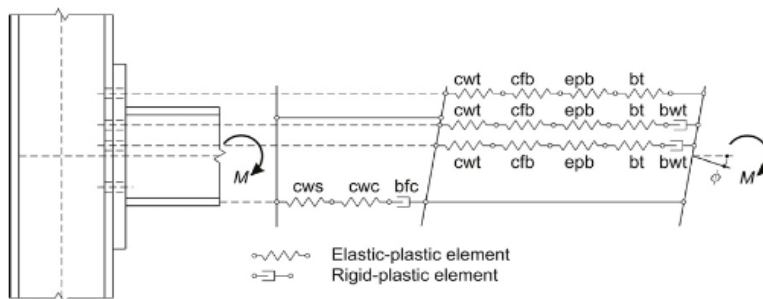


Figure 1.3: A mechanical model example [28]

1.2.1.5 Finite Element modeling of semi-rigid connections

Cost of experimental tests could be very high; thus detailed numerical modeling of the bolt, flange and web regions through accurate description of contact, friction and pretension [9-13] could be employed. Such capabilities exist in finite element programs such as ABAQUS and ANSYS, however the complex interaction of nonlinearities pose significant convergence problems, and furthermore attaining an accurate model may not be always possible even with the use of these advanced analysis techniques. In Figure 1.4 a representative 3D finite element connection model with undeformed and deformed configuration is shown [14].

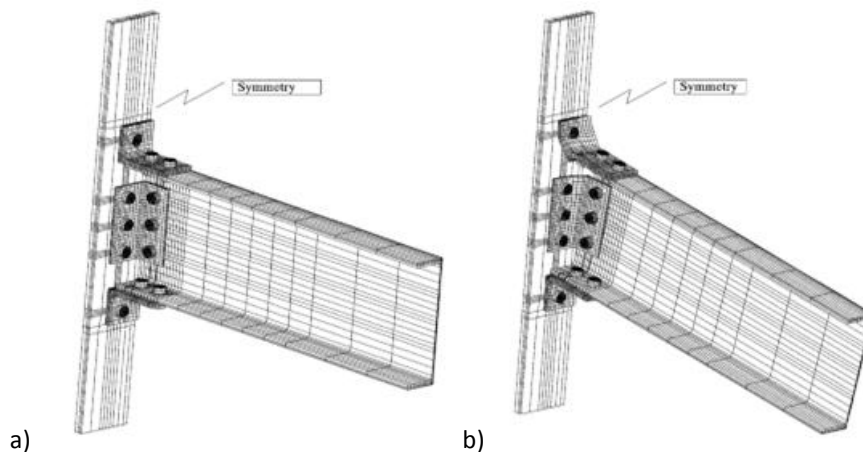


Figure 1.4: A representative 3D finite element connection model, a) undeformed configuration, b) deformed configuration [14]

1.2.2 Analyses of steel frames with semi-rigid connections

In structural analyses beam-column connections are assumed to be rigid or pinned. In other word either the relative rotation between the beam and column or the moment transferred from beam to column is zero. Since these assumptions do not reflect the reality, semi rigid behavior of the connections should be included in the analyses. Several researches [15-19] have been done in which connections were modeled as a spring attached to the end of the beam.

In the study of Lui and Chen[16] beam elements were formulated with updated Lagrangian approach which takes formation of the plastic hinges in the beam and both axial force and bending moment effects into consideration. In the formulation of this beam element, it was assumed that the member was prismatic and plane section remained plane, and thus distortion of the members was assumed to be negligible. Plasticity was assumed to exist only as a lumped value at the plastic hinge location and the remaining part of the member was linear elastic. For the moment rotation curve of the connection an exponential function was used. Figure 1.5[16] shows the deformed configuration of the beam element including connections at the ends used in that study. At the end of that paper, the researchers also carried out an analysis on the effect of connection type on the structural behavior. Figure 1.6[16] shows the effect of the connection type on moment distribution at the beam ends from that study.

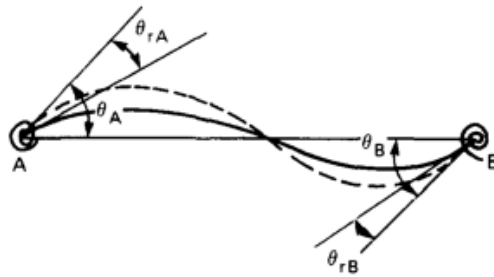


Figure 1.5: Deformed configuration of the beam element with connections [16].

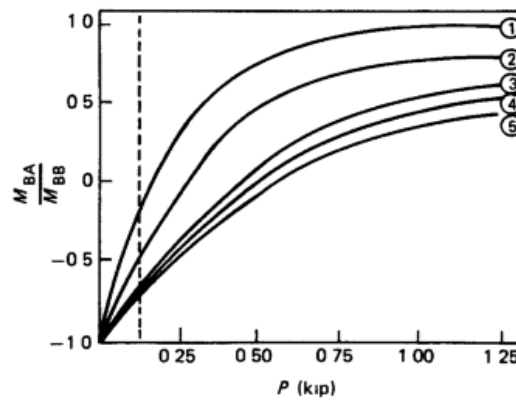


Figure 1.6: Effect of connection flexibility on moment distributions of beam end moments (1) single web angle; (2) double web angle, (3) top and seat; (4) end plates; (5) rigid [16]

In the study of Sekulovic and Salatic [17] the effect of the connection flexibility on the behavior of the structure under static loading was examined. They used a numerical model which takes both nonlinear behavior of the connection and geometric nonlinearity of the structure into consideration. The beam model is presented in Figure 1.7 [17] and has similar assumptions with the study by Lui and Chen. They ended up with the effect of the connection flexibility on the critical load. Figure 1.8 [17] shows a graphical representation of this effect from their study.

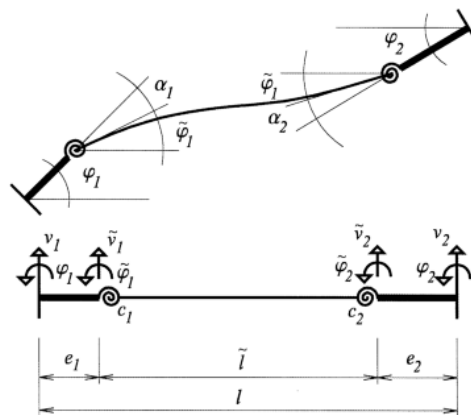


Figure 1.7: Beam model including eccentric connections [17]

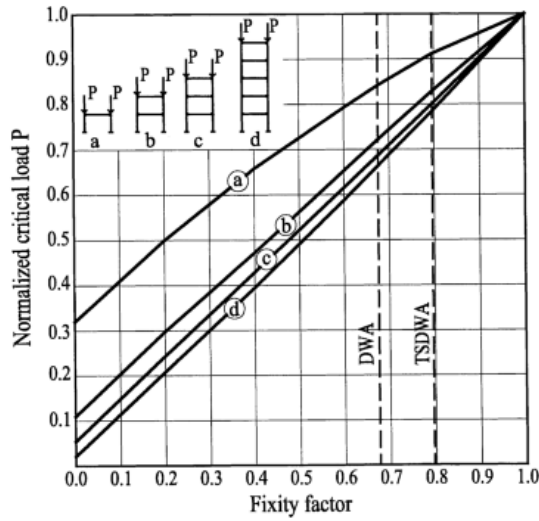


Figure 1.8: Effect of connection flexibility on the critical load [17]

After this study, in 2002 the same authors presented another study [18] in which they have examined the effects of connection flexibility on nonlinear analyses. In this case the connections were modeled as nonlinear rotational spring and a dashpot in parallel. In Figure 1.9 [18] the beam model is presented. For modeling of the moment rotation behavior of the connection under monotonic loading the three parameter power model [20] was used. The independent hardening model was adopted to simulate the inelastic connection behavior under cyclic loading and it is shown in Figure 1.10 [18]. They have concluded that the flexibility of the connection has a great importance on the nonlinear behavior of the structure. In the Table 1.1 [18] the effect of connection flexibility on the natural frequency period of the structure is shown. In this table TSDWA means Top and Seat Double Web Angle and DWA means Double Web Angle.

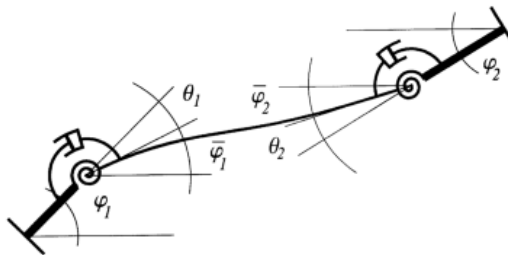


Figure 1.9: The beam model in which connections are modeled using a rotational spring and a dashpot [18]

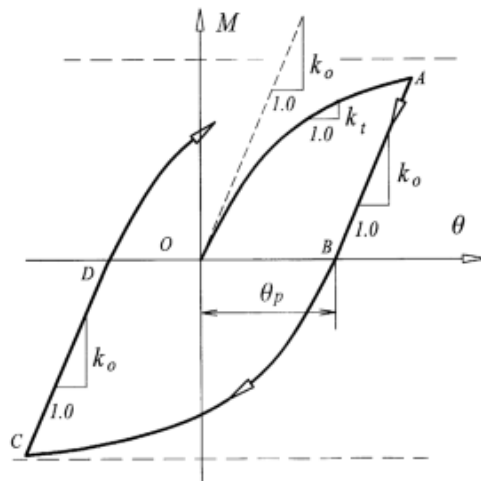


Figure 1.10: The adopted independent hardening model [18]

Table 1.1: The natural frequencies of the structure with varying type of connection [18]

Type of connection	Natural frequencies (rad/s)			Periods (s)		
	First mode	Second mode	Third mode	First mode	Second mode	Third mode
Rigid	6.328	17.523	31.116	0.993	0.359	0.202
TSDWA	5.727	16.088	28.611	1.097	0.391	0.220
DWA	4.647	13.519	24.247	1.352	0.465	0.259

Castellazzi [21] has also studied the influence of flexible joints on the response of framed structures. He has developed a second order shear deformable beam element incorporating flexibility and eccentricity of connections at the end of the beam. The element is shown in Figure 1.11, and it has similar assumptions with regards to lumping of plasticity at element ends and the remaining of the beam being linear elastic. The developed element uses second order Timoshenko's beam model. While developing the structural stiffness matrix Castellazzi condensed out the additional degrees of freedoms so that the dimension of the matrix is 6x6. At the end of his study he observed the effect of connection flexibility and eccentricity on the natural frequencies of the structure and compared them with the results of Suarez LE, Singh MP, Matheu EE [29].

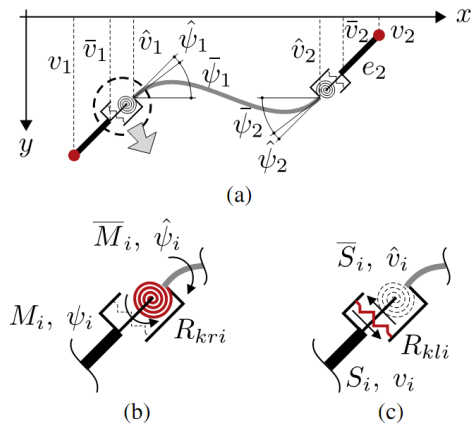


Figure 1.11: Details of beam with connectors [21]

In a very recent study by Valipour and Bradford [22], a frame element that considers spread inelasticity along element length and nonlinear semi-rigid behavior at element ends was developed. The element has been developed based on force formulation using total secant stiffness approach. Due to the use of force based formulation, a single macro element was used for capturing the response of the beam and connections together. The nonlinear response of the connection did not take into account stiffness and strength degradation and pinching effects, but they opted to use both a bilinear model with kinematic hardening and alternatively the Ramberg–Osgood model shown in Figure 1.12. The connection region considered both moment-rotation behavior and axial force-deformation behavior, thus contained both rotational and translational springs. At the end of the study analyses were performed by using the developed frame elements. Firstly a 6-storey then 5-storey frames were examined. Then the results obtained by using their elements have been compared with ABAQUS results. Also some progressive collapse analyses cases have been examined as an extension for the use of their developed frame elements in the paper.

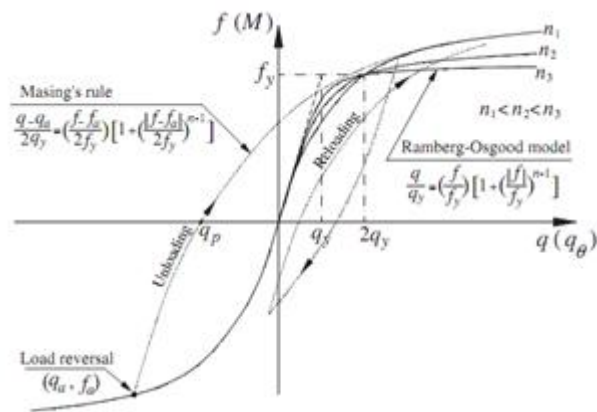


Figure 1.12: Ramberg–Osgood model [22]

1.3 Organization of thesis

In this thesis firstly a macro element based on force formulation is developed to incorporate our model into structural analysis. Then, a moment-rotation model for semi-rigid connections is developed. Eventually, the proposed models are tested by using already available experimental data.

The presentation of this thesis has been divided into five chapters including this chapter.

In Chapter 2 a macro element which is based on force formulation and includes distributed inelasticity and incorporates nonlinear connectors at any location along element length is developed.

In Chapter 3 an existing uniaxial model available in Fedeaslab and OpenSees finite element programs is presented. Modifications to calibrate the existing model have been explained.

In Chapter 4 verification of the developed model is presented via experimental data available in the literature.

Finally, in Chapter 5 summary and conclusions of the thesis work are presented. Furthermore, future research recommendations related to the modeling of semi-rigid connections in the analysis of framed structural systems are stated.

CHAPTER 2

DEVELOPMENT OF NONLINEAR FRAME ELEMENT WITH SEMI-RIGID CONNECTORS

The derivation of frame finite elements could be pursued either with displacement based or force based approaches, where the latter is also categorized under mixed methods. Formulation of a nonlinear macro element model with semi-rigid connectors through the use of displacement based finite elements requires increased number of meshing and thus the use of several degrees of freedom. In a recent study, Saritas and Soydas [23] has shown for small and large structural systems that increased element numbers and degrees of freedom as a result of the use of displacement based approach results in significant increases in computation times when compared with the use of force-based approaches. In general, if the spread of plasticity along a member is sought, at least 8 to 16 elements are necessary to accurately capture the nonlinear behavior with displacement based approach. With the introduction of semi-rigid connectors, as many more zero-length spring elements will be required. Development of a macro element model with displacement based approach in this regards would not be a truly novel contribution since it would be just the assembly of the responses of several elements with the use of finite element software and by attaching rotational springs to the ends. Despite this fact, there is still effort that should be spent in accurately capturing the cyclic behavior of semi-rigid connectors as discussed in the next chapter, and such a model should be implemented and used as part of a frame finite element analysis program nevertheless.

Formulation of the nonlinear frame element with semi-rigid connectors in this thesis is based on the fact that force interpolation functions are used in predicting the element response. The element is composed of continuous element portions with discontinuities arising due to the presence of zero-length rotational springs. Kinematics of the continuous portion of the frame element follows Euler-Bernoulli Beam Theory (EBT) assumptions, in which plane sections before deformation remain plane after deformation. As part of this theory, shear deformations are neglected, and thus element response is due to the presence of normal stress along element length. Nonlinear response of the continuous portion of the element is aggregated from the monitoring of the responses of several control sections along element length, and furthermore at each section, the response is assembled through fiber discretization of the section.

The formulation of the element starts with the calculation of axial force $N(x)$ and bending moment $M(x)$ from basic element forces q_1 , q_2 and q_3 (Figure 2.1). In the absence of inter element loads, these internal forces can be simply calculated with statics knowledge as follows:

$$\begin{matrix} s \\ x \end{matrix} = \begin{matrix} N \\ M \end{matrix} \begin{matrix} x \\ x \end{matrix} = \begin{matrix} \frac{x}{L} - 1 \\ 1 \end{matrix} \begin{matrix} q_1 \\ q_2 \end{matrix} + \begin{matrix} \frac{x}{L} \\ 0 \end{matrix} q_3 \quad \mathbf{2.1}$$

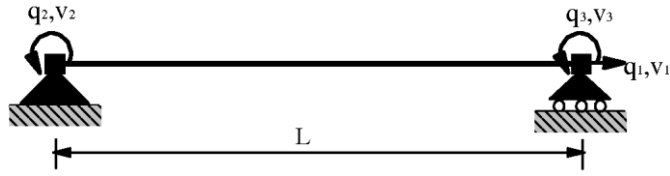


Figure 2.1: Basic Forces and Deformation for Beam Element

Above equation can be extended to the presence of distributed uniform element loads w_x and w_y applied in the axial and transverse directions, respectively, and can be written as:

$$\mathbf{s}(x) = \mathbf{b}(x) \mathbf{q} + \mathbf{s}_p(x) \quad 2.2$$

where \mathbf{q} is the vector of basic element forces, $\mathbf{b}(x)$ represents the force-interpolation functions and can be regarded as an equilibrium transformation between section forces $\mathbf{s}(x)$ and basic forces \mathbf{q} , and the particular solution $\mathbf{s}_p(x)$ is due to uniform loads w_x and w_y , where these are all given as:

$$\mathbf{q} = \begin{bmatrix} q_1 \\ q_2 \\ q_3 \end{bmatrix}; \quad \mathbf{b}(x) = \begin{bmatrix} 1 & 0 & 0 \\ 0 & \frac{x}{L} - 1 & \frac{x}{L} \end{bmatrix} \quad 2.3$$

$$\mathbf{s}_p(x) = \begin{bmatrix} L(1 - \frac{x}{L}) & 0 \\ 0 & \frac{L^2}{2} \frac{x^2}{L} - \frac{x}{L} \end{bmatrix} \begin{bmatrix} w_x \\ w_y \end{bmatrix} \quad 2.4$$

Principle of virtual forces necessitate the equality between virtual element end forces $\delta \mathbf{q}$ multiplied with real element deformations \mathbf{v} to be calculated from the integration of virtual section forces $\delta \mathbf{s}$ multiplied with real section deformations \mathbf{e} . This equality is expressed in the following equation,

$$\delta \mathbf{q}^T \mathbf{v} = \int_L \delta \mathbf{s}^T(x) \mathbf{e}(x) dx \quad 2.5$$

where section deformations are written as:

$$\mathbf{e} = \begin{bmatrix} \epsilon_a \\ \kappa \end{bmatrix} \quad 2.6$$

Introduction of the section interpolation functions from above equations and with the fact that virtual forces are arbitrary, element end forces are calculated from the section deformations as follows:

$$\mathbf{v} = \int_L \mathbf{b}^T(x) \mathbf{e}(x) dx \quad 2.7$$

Element flexibility matrix \mathbf{f} can be calculated from above equation by considering partial differentiation with respect to element end forces:

$$\mathbf{f} = \frac{\partial \mathbf{v}}{\partial \mathbf{q}} = \frac{\partial}{\partial \mathbf{q}} \int_L \mathbf{b}^T(x) \mathbf{e}(x) dx = \int_L \mathbf{b}^T(x) \frac{\partial \mathbf{e}(x)}{\partial \mathbf{s}(x)} \frac{\partial \mathbf{s}(x)}{\partial \mathbf{q}} dx \quad 2.8$$

$$\mathbf{f}_{s(x)} \mathbf{b}(x)$$

where \mathbf{f}_s is the section flexibility matrix that can be calculated from the inversion of the section stiffness matrix \mathbf{k}_s .

At this point in the element formulation, continuous integrals written above will be discretized and furthermore the presence of semi-rigid connectors will be introduced through the following extended version of above equation for the calculation of element end deformations:

$$\mathbf{v} = \mathbf{v}_{Elem} + \mathbf{v}_{Con} \quad 2.9$$

$$\mathbf{v}_{Elem} = \sum_{i=1}^{nIP} \mathbf{b}^T(x_i) \mathbf{e}_i wIP_i ; \text{ and } \mathbf{v}_{Con} = \sum_{i=1}^{nSC} \mathbf{b}^T(x_i) \Delta_{SC,i} \quad 2.10$$

where nIP is the total number of monitoring sections used for the calculation of the nonlinear response of the continuous portion of the element and nSC is the total number of semi-rigid connectors present along the element; wIP is the integration weight corresponding to that integration location, and eventually $\Delta_{SC} = \delta \theta^T$ is the vector of semi-rigid connector deformations composed of axial deformation δ and rotation θ of a connector.

Element flexibility matrix is similarly discretized as follows:

$$\mathbf{f} = \mathbf{f}_{Elem} + \mathbf{f}_{Con} \quad 2.11$$

$$\mathbf{f}_{Elem} = \sum_{i=1}^{nIP} \mathbf{b}^T(x_i) \mathbf{f}_{s_i} \mathbf{b}(x_i) wIP_i ; \text{ and } \mathbf{f}_{Con} = \sum_{i=1}^{nSC} \mathbf{b}^T(x_i) \mathbf{f}_{SC,i} \mathbf{b}(x_i) \quad 2.12$$

The use of Gauss-quadrature or Gauss-Lobatto quadrature integration points with number of integration points nIP selected as 5 results in an accurate nonlinear behavior for the continuous part [24]. With regards to the nonlinear behavior of semi-rigid connectors, the current study will focus on only the presence of flexibility and nonlinear behavior for the rotational component of semi-rigid connectors, thus axial behavior is assumed as rigid with infinite strength. With this assumption, deformation and flexibility due to the connector parts can be modified as follows:

$$\mathbf{v}_{Con} = \begin{matrix} 0 \\ \frac{n_{SC}}{L} x_i - 1 \\ \frac{x_i}{L} \end{matrix} \theta_{SC,i} \quad 2.13$$

$$\mathbf{f}_{Con} = \begin{matrix} 0 \\ \frac{n_{SC}}{L} x_i - 1 \\ \frac{x_i}{L} \end{matrix} \frac{\partial M}{\partial \theta}^{-1}_{SC,i} \begin{matrix} 0 \\ \frac{x_i}{L} - 1 \\ \frac{x_i}{L} \end{matrix} \quad 2.14$$

Linear elastic prismatic beam without semi-rigid connectors:

For demonstration of the resulting integrals, it is now assumed that semi-rigid connectors are not present. Flexibility matrix of the element can be specialized for the case of linear elastic prismatic beam with constant elastic modulus E , cross-sectional area A and moment of inertia I . If the element axis is located at the centroidal axis, then the section flexibility matrix is written as follows:

$$\mathbf{f}_s x = \begin{matrix} \frac{1}{EA} & 0 \\ 0 & \frac{1}{EI} \end{matrix} \quad 2.15$$

Flexibility of the continuous portion of the element can be thus obtained in closed form to get the well-known matrix in structural analysis:

$$\mathbf{f} = \int_0^L \mathbf{b}^T x \mathbf{f}_s x \mathbf{b} x dx = \begin{matrix} \frac{L}{EA} & 0 & 0 \\ 0 & \frac{L}{3EI} & -\frac{L}{6EI} \\ 0 & -\frac{L}{6EI} & \frac{L}{3EI} \end{matrix} \quad 2.16$$

where the inverse of the flexibility matrix yields the element stiffness matrix for the simply supported beam:

$$\mathbf{k} = \mathbf{f}^{-1} = \begin{matrix} \frac{EA}{L} & 0 & 0 \\ 0 & \frac{4EI}{L} & \frac{2EI}{L} \\ 0 & \frac{2EI}{L} & \frac{4EI}{L} \end{matrix} \quad 2.17$$

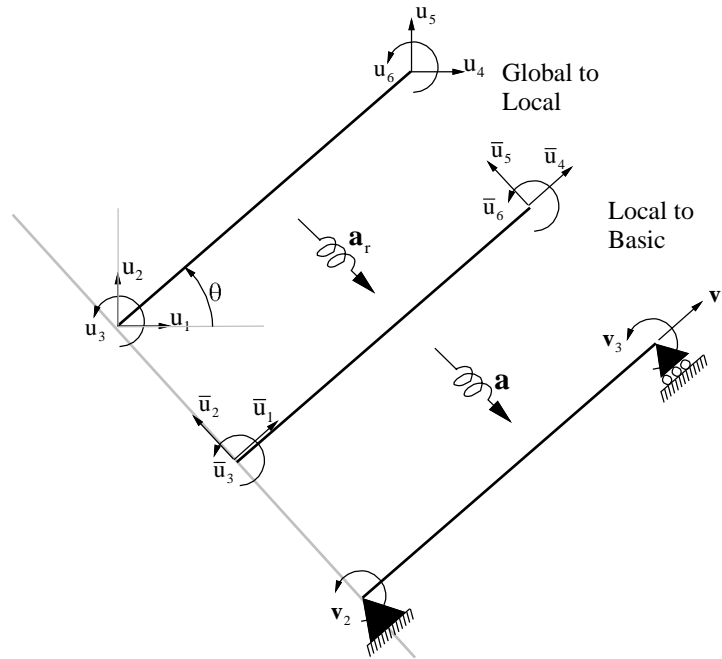


Figure 2.2: Transformation of Element Displacements to Deformations

The stiffness matrix of the two-node frame element in local coordinate system can be further calculated through the inclusion of rigid body modes by the following transformation between basic deformations and displacements in local coordinates shown in Figure 2.2.

$$\mathbf{v} = \mathbf{a} \mathbf{u}; \text{ and } \mathbf{a} = \begin{bmatrix} -1 & 0 & 0 & 1 & 0 & 0 \\ 0 & 1/L & 1 & 0 & -1/L & 0 \\ 0 & 1/L & 0 & 0 & -1/L & 1 \end{bmatrix} \quad 2.18$$

This transformation gives the stiffness matrix in local coordinates as:

$$\mathbf{k} = \mathbf{a}^T \mathbf{k} \mathbf{a} = \begin{bmatrix} EA/L & 0 & 0 & -EA/L & 0 & 0 \\ 0 & 12EI/L^3 & 6EI/L^2 & 0 & -12EI/L^3 & 6EI/L^2 \\ 0 & 6EI/L^2 & 4EI/L & 0 & -6EI/L^2 & 2EI/L \\ -EA/L & 0 & 0 & EA/L & 0 & 0 \\ 0 & -12EI/L^3 & -6EI/L^2 & 0 & 12EI/L^3 & -6EI/L^2 \\ 0 & 6EI/L^2 & 2EI/L & 0 & -6EI/L^2 & 4EI/L \end{bmatrix} \quad 2.19$$

Transformation of the stiffness matrix from local to global coordinates shown in Figure 2.2 is obtained with simple rotational transformation and can be found in standard textbooks in matrix structural analysis.

Implementation of the Proposed Frame Element in a Finite Element Program

The proposed frame element with semi-rigid connectors is implemented in a standard finite element software package that assumes that the element response is composed of resisting forces and

stiffness matrix, where in this regards the element formulation should appear to be displacement-based to the program.

A general finite element program tries to find the equilibrium between applied forces \mathbf{P}_{app} and resisting forces \mathbf{P}_r written as such:

$$\mathbf{P}_{app} - \mathbf{P}_r(\mathbf{U}) = \mathbf{0} \quad 2.20$$

Since above equation is nonlinear in general, linearization is necessary, thus resulting in the following incremental solution with Newton-Raphson iterations:

$$\Delta \mathbf{U} = \mathbf{K}^{-1} \mathbf{P}_{app} - \mathbf{P}_r(\mathbf{U}_i) \quad 2.21$$

Initial guess for displacements can be simply assumed as zero, i.e. $\mathbf{U}_0 = \mathbf{0}$.

Given the state of displacements at iteration counter i , element nodal displacements in global coordinates are readily available, thus element local displacements are calculated, and then element basic deformations are in turn computed as $\mathbf{a} \mathbf{u}$ as demonstrated in an above equation (Eqn. 2.18).

Assuming that the computed element deformations are imposed on the force-based element, it can be written that $\mathbf{v} = \mathbf{a} \mathbf{u}$.

The basic element deformations of the force-based element are obtained through independent element forces \mathbf{q} by a nonlinear equation as $\mathbf{v} = \mathbf{v}(\mathbf{q})$. The imposed deformations \mathbf{v} and element response \mathbf{v} should match i.e.

$$\mathbf{v} - \mathbf{v}(\mathbf{q}) = \mathbf{0} \quad 2.22$$

Solution of above equation is only possible through linearization as depicted below:

$$\mathbf{v} - \mathbf{v}(\mathbf{q}_i) + \frac{\partial \mathbf{v}}{\partial \mathbf{q}}_{\mathbf{q}_i} (\mathbf{q} - \mathbf{q}_i) = \mathbf{0} \quad 2.23$$

This results in the following incremental update of the element end forces:

$$\Delta \mathbf{q} = \mathbf{f}_i^{-1} \mathbf{v} - \mathbf{v}(\mathbf{q}_i) \quad 2.24$$

With new update on element end forces, new section forces can be calculated through the equilibrium transformation presented before, i.e. $\mathbf{b} \mathbf{x} \mathbf{q} + \mathbf{s}_p \mathbf{x}$.

The response of the monitoring sections and the semi-rigid connectors bases on a rather straight forward constitutive relation that is deformation driven, i.e. $s(e)$ and $M(\theta)$, respectively; thus the responses are the section forces (axial force, bending moment, etc...) and the section stiffness matrix. This necessitates the compatibility between the section forces calculated from element end forces with the responses of the sections for a current level of deformation, i.e. the response of the sections are as such:

$$\mathbf{b} \times \mathbf{q} + \mathbf{s}_p \times x = \mathbf{s}(e) \quad 2.25$$

Satisfaction of above equality requires once again linearization as shown below:

$$\mathbf{b} \times \mathbf{q}_i + \mathbf{s}_p \times x = \mathbf{s} e_i + \frac{\partial \mathbf{s}}{\partial e} e_i \Delta e \quad 2.26$$

This results in the following incremental update on deformations:

$$\Delta e = \mathbf{k}_{s,i}^{-1} \mathbf{b} \times \mathbf{q}_i + \mathbf{s}_p \times x - \mathbf{s}(e) \quad 2.27$$

Similarly, the update of rotation values for a semi-rigid connector located at x can be calculated as:

$$\Delta \theta = \frac{\partial M}{\partial \theta}^{-1} \left[\frac{x}{L} - 1 \right] q_{2,i} + \frac{x}{L} q_{3,i} + \frac{L^2}{2} \left[\frac{x^2}{L} - \frac{x}{L} \right] w_y - M \theta_i \quad 2.28$$

Once new section deformations and connector rotations are available, responses are easily obtained through constitutive relations, and then the element response is in turn calculated through the equations presented above. The response of the element will be eventually the stiffness matrix (that is the inverse of the flexibility matrix) and the element resisting forces (that are the final values of the element end forces \mathbf{q}).

CHAPTER 3

A HYSTERESIS SECTION MODEL FOR SEMI-RIGID CONNECTIONS

3.1 Presentation of hysteresis uniaxial model

Experiments available in the literature show that under cyclic loading it is reasonable to characterize the behavior of steel connections with hysteretic loops incorporating strength and stiffness degradation. Traditionally multi-parameter mathematical models have been developed to achieve this task; however, especially under cyclic loading the behavior is quite complex due to some phenomena named as pinching that results from material and geometric nonlinearities in the connection. It should be emphasized that the development of a multi-parameter model alone would not be a complete work without calibrating those parameters to reproduce moment rotation curves for different connection topologies.

Several simplified mathematical models are available in literature; namely linear, bilinear, tri-linear or more general multi-linear and nonlinear, where the first two models are inadequate in reflecting the cyclic behavior in an accurate manner. In this study, a quadra-linear model is preferred. Selected model bases on the same tri-linear model present in both Fedeaslab and OpenSees finite element programs. Extension to quadra-linear behavior with added parameters was needed in order to better capture pinching and residual moment capacities in the connection. In the following sections first pinching phenomena will be clearly explained, and then the existing base model in Fedeaslab and the modified model will be thoroughly described.

3.2 Pinching

Pinching can be described as a reduction of member stiffness upon reloading, and is a common characteristic behavior of concrete plastic zones and steel connections under cyclic loading. The behavior is not only observed in moment-rotation relation but also in shear or axial force-deflection relations, as well (Figure 3.1). The sources of pinching are numerous and vary according to the type of loading and material.

The major reason of pinching in steel connections is the changing shape of the bolt holes on the beam web from circle to ellipse due to high shear forces transferred with bolts. In other words local bearing failure of the holes leads to pinching. Since the bearing takes place in nonlinear range, the deformations of bolt holes are permanent. When a load reversal is introduced, the bolts move freely in their holes and this leads to significant degradation of stiffness. After bolts start to contact with other sides of the holes, the stiffness start to increase gradually. When a full contact is gained again the stiffness increases suddenly. This implies that pinching leads to rotation shifting in the material behavior which means nothing is lost in terms of capacity. However, since pinching leads to get same moment in higher rotations, failure occurs due to excessive rotation this time. This is what makes pinching responsible for decreasing capacity of the connection. The phenomenon can be observed in a bigger scale by considering the contact of beam flange to the column flange of a web angle connection after going through a very high rotation. Since other structural elements cannot undergo such a high rotation, the increasing capacity of connection at this level of rotation may not be

effective. From these observations it can be concluded that pinching occurs less in welded connections. However, it is also possible to observe pinching in bolted-welded web angle connections in which angles are welded to the beam web and bolted to the column flange. The reason of pinching in the last connection type is different than the one observed in bolted-bolted connections in which angles are bolted to both the beam web and the column flange. For this case, permanent elongation of the bolts connecting the angle and column flange is now responsible for pinching only. Remaining mechanism can be deduced in a similar way for the one explained earlier.

The start and end locations of pinching and its amount present on the moment-rotation curve varies with the connection types and geometry. For this reason, defining the influence of each factor on pinching is a difficult task and requires significant effort. In this respect, the developed function in Matlab permits the user to easily change the pinching parameters in order to better capture the experimentally tested behavior of a selected connection topology. A large pool of parameters is run in Matlab, and the best fit in terms of energy dissipation is considered as the selected parameter for each experiment. In a future study, these calibrated parameters could be used as a data bank for the suggestion of pinching parameters according to different connection types.

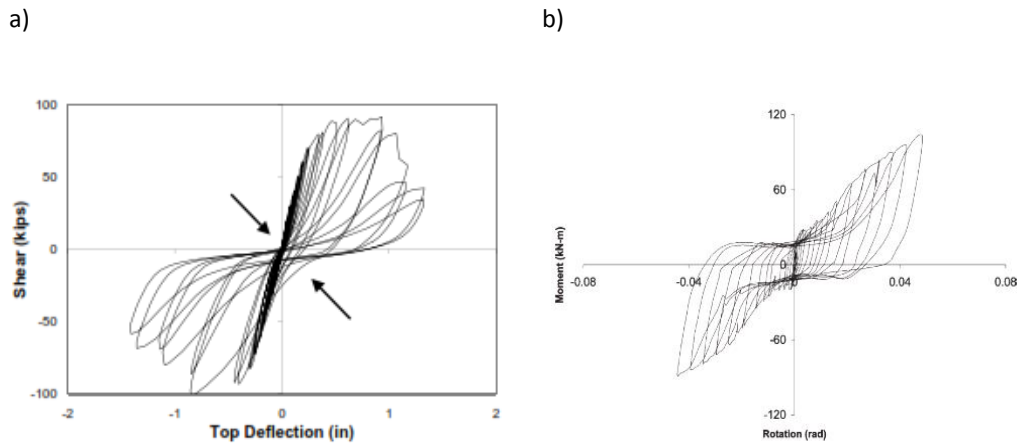


Figure 3.1: Pinching in the different behavior of different material a) shear force–deflection relation of a concrete member [30]; b) moment-rotation relation of steel connection [3]

3.3 Existing model

The tri-linear backbone curve of the existing model is shown in Figure 3.2. Yielding and ultimate moments can be determined from steel specifications and change according to type of the connection. The unloading stiffness has been taken as equal to initial stiffness which is reasonable when considering experimental tests (See Figure 3.3).

In Figure 3.4 positive loading-unloading part of the model is shown in detail. The moment value is calculated in each rotation increment as follows:

$$momnt = momntP + drot * stiff \quad 3.1$$

where $momntP$ and $rotP$ refer to previous moment and rotation, respectively, and $momnt$ and rot are the current respective values. $Drot$ is the rotation increment which relates $rotP$ and rot according to the following equation:

$$rot = rotP + drot \quad 3.2$$

$Stiff$ is the stiffness of the current linear part of the model. $Rotpu$ is the point where un-loading line intersects with the rotation axis. In other words, it is the point where positive un-loading finishes and negative re-loading starts and it is calculated as follows:

$$rotpu = rotmax - \frac{maxmom}{E1p} \quad 3.3$$

In Eqn 3.3 $rotmax$ is the maximum rotation value obtained from previous cycles and it is updated in each cycle. $Maxmom$ is, however, not the maximum moment value but the moment value at maximum rotation, $rotmax$.

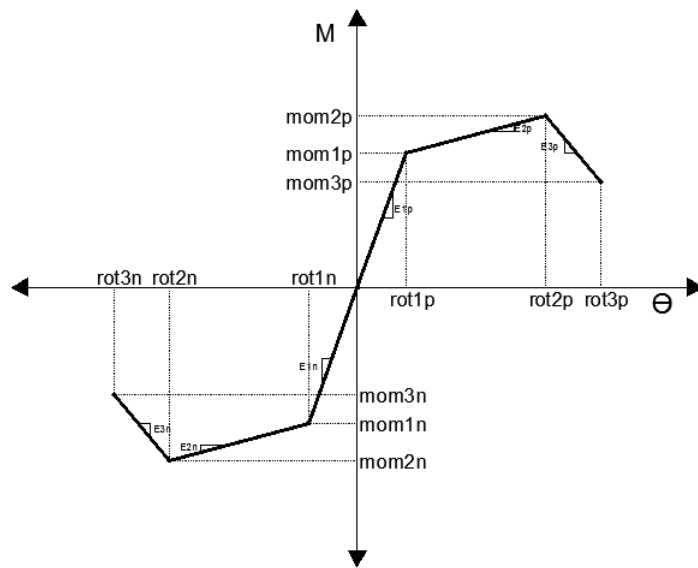


Figure 3.2: Backbone curve of used tri-linear model

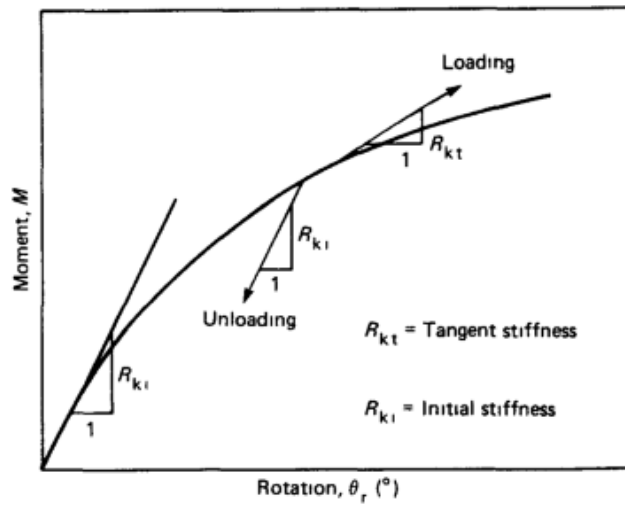


Figure 3.3: Configuration of initial, tangent and unloading stiffness values of connections [16]

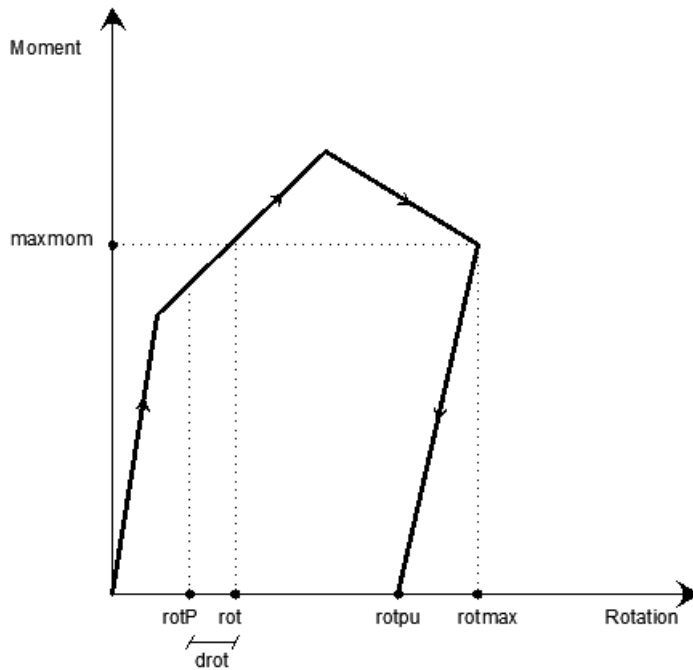


Figure 3.4: Positive loading and un-loading of the model

In Figure 3.5 positive re-loading behavior of the model is shown. As in the case of $rotpu$, $rotnu$ is the point where negative un-loading finishes and positive re-loading starts. Re-loading is demonstrated as the line A-B which means that it starts at point A ($rotnu$) and goes toward the point B. Point B is called as the target point since the re-loading line must go toward itself with or without pinching and its coordinates are $rotmax$ and $maxmom$. The slope of the line A-B, stiffness of the re-loading part, can be calculated by the following equation.

$$K_{AB} = \frac{maxmom}{rotmax - rotnu}$$

3.4

After reaching the target point, re-loading part continues toward to point D.

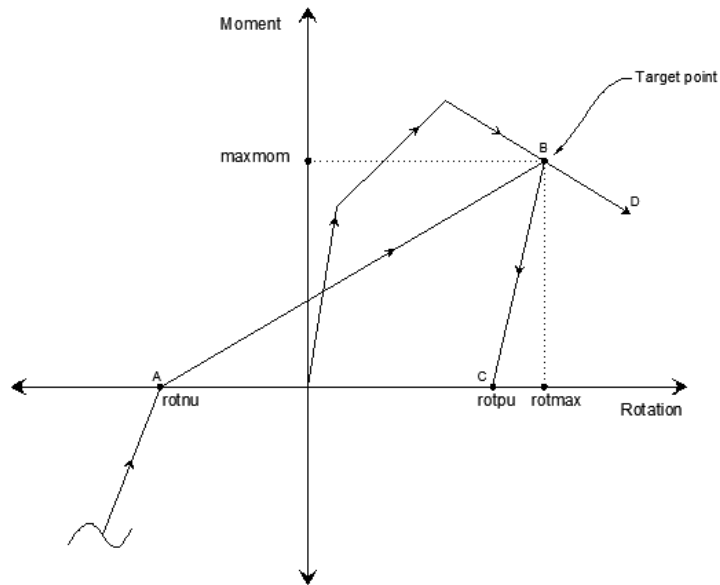


Figure 3.5: Positive re-loading of the model

3.3.1 Implementation of pinching into current model

A quantitative configuration of the pinching of the model is shown in Figure 3.6. In the current model the pinched re-loading part is represented as a bi-linear curve. Although this approach decreases the accuracy of the model in terms of capturing energy dissipation, it still provides sufficient effects in terms of modeling pinching behavior observed in several types of structural members. For a more accurate representation, it is better to use a curvilinear relationship. In addition to this, since the model is composed of several linear parts the implementation of a curvilinear part to the program would affect the consistency of the program. In other words stiffness updating would be needed in each rotation increment whereas in the case of linear parts stiffness remains constant between the two defined rotation values. As a result using a bi-linear reloading rule instead of curvilinear one is at least as reasonable as using tri-linear model instead of non-linear one.

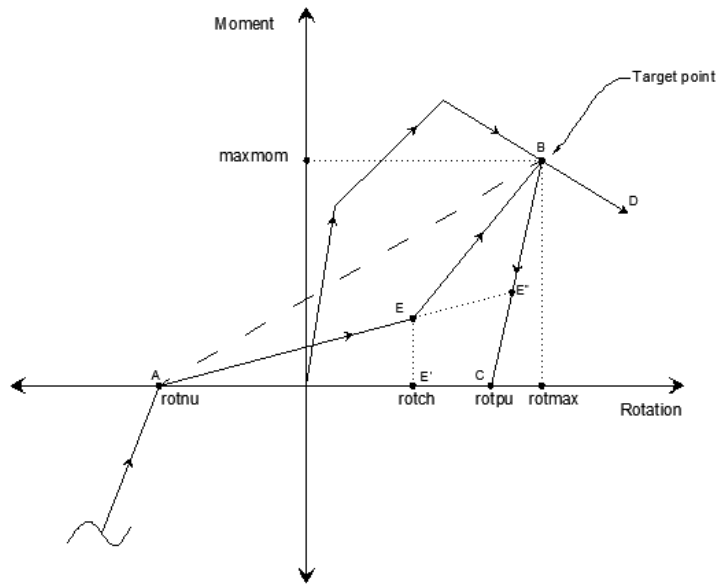


Figure 3.6: Configuration of pinching behavior of the model

In Figure 3.6 it can be seen that the two linear segments of the re-loading part intersect at the rotation value called as *rotch* (Point E'). Location of this point varies according to the connection type and is hard to relate with each connection type. Furthermore the stiffness of the pinched part (slope of the line A-E) may change. Thus, defining the location of the point E is necessary and adequate to define the two other required values; i.e. location of point E' and slope of the line A-E. Once the location of the pinching point (point E) is defined, the location and slope of the remaining segment (line E-B) will be defined automatically. So it is reasonable to allow the user to control the location of the pinching point and this was achieved by two parameters in the current model. One of these parameters, *pnchx*, controls the location of the pinching point on the rotation axis, and the other parameter *pnchy* controls location of the pinching point on both rotation and moment axes. However, the formulation of the location of point E is derived with these parameters in such a way that the slope of the line A-E cannot be larger than the slope of the line A-B (stiffness in un-pinched re-loading). Other restriction is that the slope of the line E-B must be between the slope of line A-B and line C-B. In other words the location of the point E must be in the area defined by angle between the line A-B and line C-B. The second restriction is so reasonable that it prevents the formation of negative energy loops that are unrealistic (See Figure 3.7).

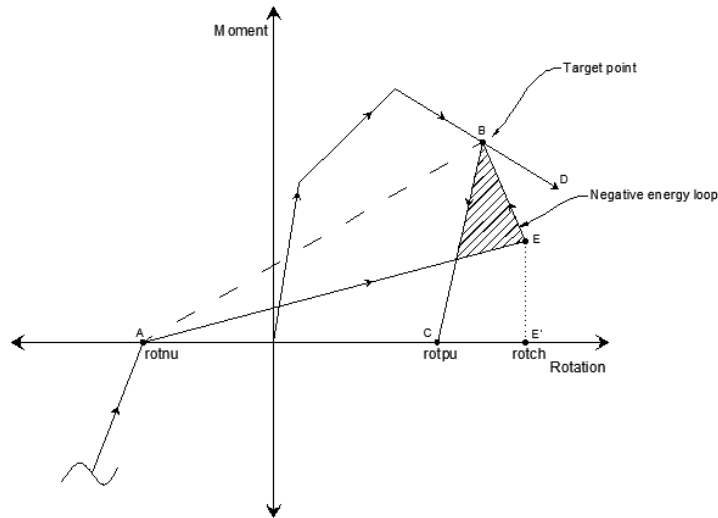


Figure 3.7: Configuration of negative energy loop

The effects of the two parameters, namely $pnchx$ and $pnchy$, to the location of the pinching point (point E) can be explained as follows. Setting the value of $pnchy$ equal to zero makes the slope of the line A-E equal to zero. In other words point E will be on the rotation axis. In this case the location of the point E takes a value between the points $rotnu$ and $rotpu$. Then the value of $pnchx$ defines the exact location of the point E. If value of $pnchx$ is zero, then point E overlaps with the point A. On the other hand setting the value of $pnchx$ equal to one, in the case of value of $pnchy$ is equal to zero, makes the point E overlap with the point C. Parameters set as such gives 'fully pinching' condition in this model. On the other hand when the parameter $pnchy$ takes a value of 1 the slope of the line A-E will be equal to the slope of line A-B, which means that no pinching occurs. In this case the value of $pnchx$ becomes irrelevant. It is obvious that a value between zero and 1 set for $pnchx$ and $pnchy$ gives a result between the two extreme cases explained above. In Figure 3.8 and Figure 3.9, effects of the use of different $pnchx$ and $pnchy$ value combinations on the pinching behavior are shown.

The implementation of the cases explained above is as follows:

- if $rotnu \leq rot \leq rotch$ then $stiff = K_{AD}$ and $momnt = momntP + stiff * drot$
- if $rotch \leq rot$ then $stiff = K_{DB}$ and $momnt = momntP + stiff * drot$

These rules are valid as long as rotation increment is greater than zero which means that no unloading takes place. In case of un-loading in the pinching region ordinary un-loading rules are valid.

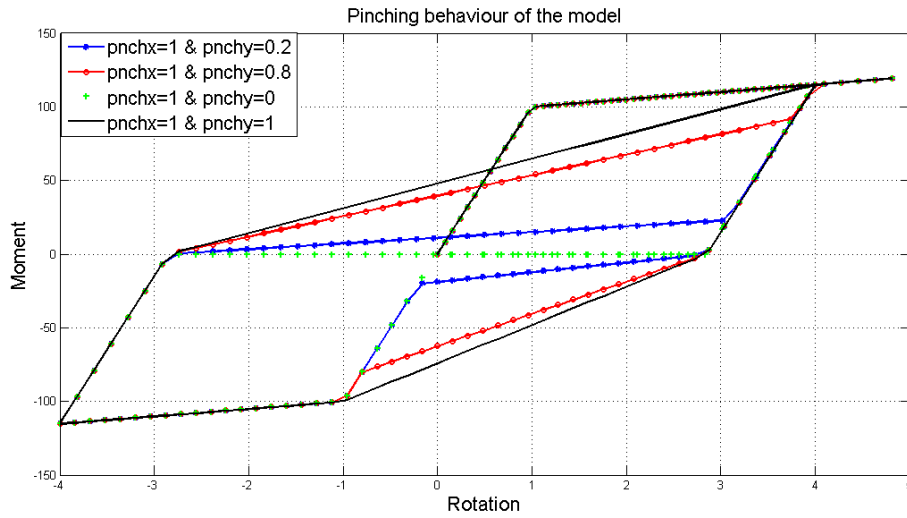


Figure 3.8: Effect of pnchy parameter with constant pnchx

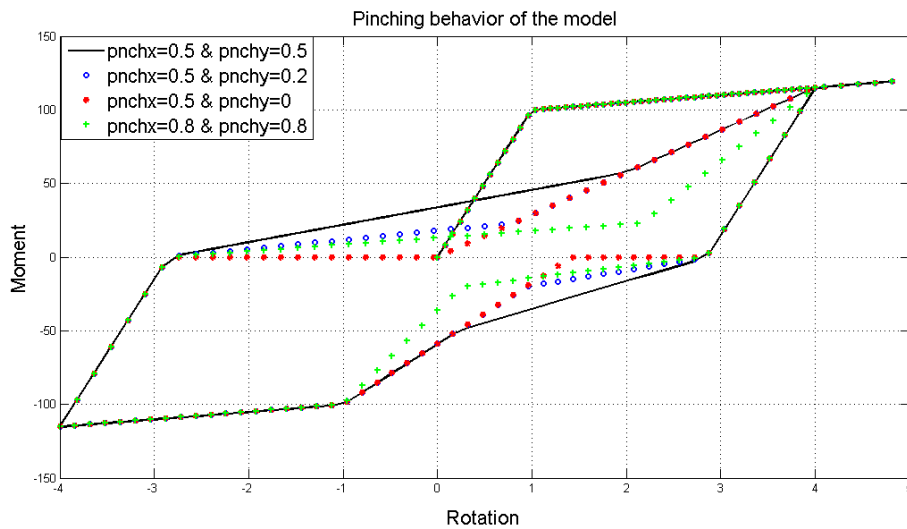


Figure 3.9: Effects of pnchx and pnchy parameter on the behavior

3.4 Modified model

As it was mentioned earlier, in steel bolted connections pinching results from permanent deformations of bolt holes that change the shape of the holes from circle to ellipse (See Figure 3.10). In the experiments in which pinching governs clearly it is also seen that the stiffness degradation due to pinching is observed at a point a bit far from zero-moment crossing (See Figure 3.11). This means that the stiffness of the un-loading branch remains same up to a moment value in the re-loading region. This moment value can be called as residual moment and used to determine the starting point of pinching.



Figure 3.10: Deformed shape of the bolt holes [25]

In the current model by assigning the $pnchx$ value smaller than zero it is possible to obtain a residual moment. However adjusting this parameter to get a required residual moment is a bit difficult. In addition to this, in this case (in the case of negative $pnchx$) the pinching mechanism of the model changes in such a way that the results are difficult to adapt with an experimental result. So an easier residual moment rule is adapted to the model. In this modification the user is allowed to define the residual moment value. Then this residual moment value is transformed to a rotation value. In other words, since the program algorithm is based on rotation values, the rotation value of the point at which the residual moment is reached (point A' in Figure 3.12) is accepted as the starting point of pinching and can be determined by the following equation

$$rotnumod = rotnu + \frac{momrestp}{E1n} \quad 3.5$$

where, $rotnumod$ = rotation value at the starting point of pinching,

$E1n$ = negative un-loading stiffness which remains same up to $rotnumod$,

$momrestp$ = positive residual moment.

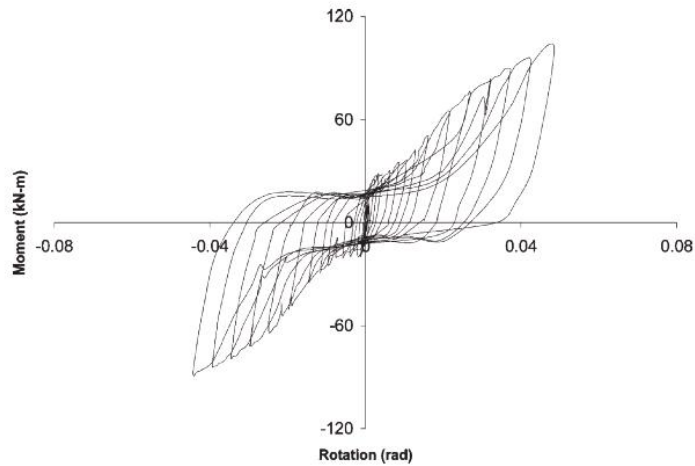


Figure 3.11: Experimental residual moment behavior [3]

In the modified model, this residual moment value is also used as a limiting value for the value of $maxmom$. In other words, if the stiffness of the any branch of the positive envelope curve is smaller than zero, the moment can decrease up to this residual moment value and then remains constant (See Figure 3.12). This limitation is applied by calculating the rotation value of point D, $rotlim$. In the original model this limiting moment value is zero instead of residual moment and it is the point D' instead of D that is used to determine the value of $rotlim$.

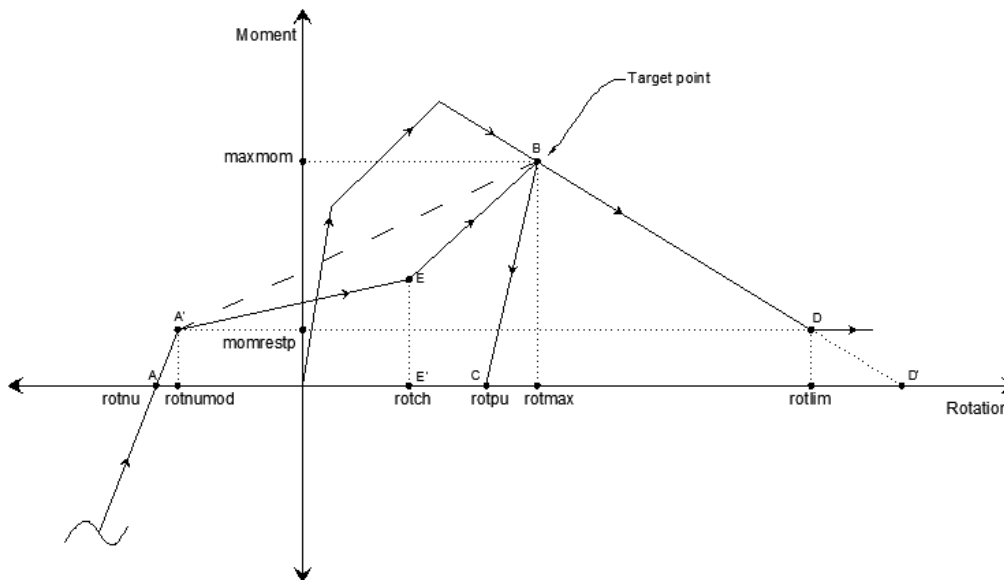


Figure 3.12: Residual moment behavior of the modified model

Other modification introduced to the model is based on an observation that in some cases the residual moment gets smaller as load cycles get larger (See Figure 3.13). This modification is arranged by introducing a slope value, K_{tp} , which is the slope of the line passing through a point on

the moment axis. This point is selected as the point of residual moment on the moment axis (See Figure 3.14). This slope value Ktp is controlled by the user since it varies according to experimental results. In this case a new variable called as $momrestpp$ is introduced which is changing according to parameters $momrestp$ and Ktp and are calculated by below equation (Eqn 3.6). In Figure 3.14 it can also be noticed that as cycles get larger the residual moment can take negative values which is reasonable when considering experimental results (See Figure 3.15).

$$momrestpp = \frac{E1n * (Ktp * rotnu + momrestp)}{E1n - Ktp} \quad 3.6$$

From Eqn 3.6 it can be noticed that the value of $momrestpp$ changes in each cycle since it depends on variable $rotnu$ which is also changing in each cycle. Finally a plot output of the modified program is shown in Figure 3.16 for the demonstration of the complete behavior of the proposed model.

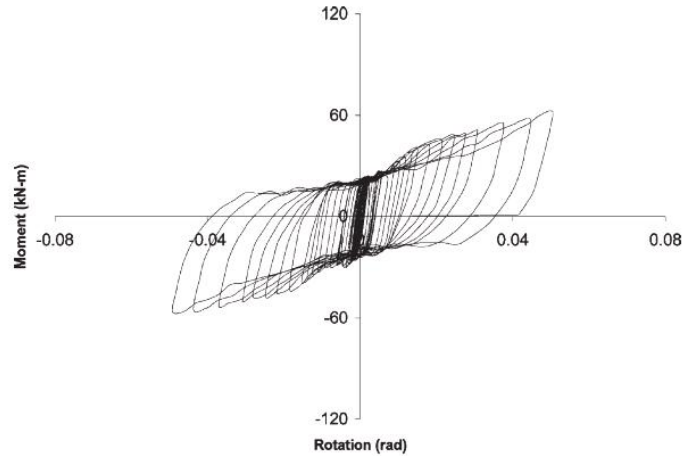


Figure 3.13: Experimental example of decreasing residual moment [3]

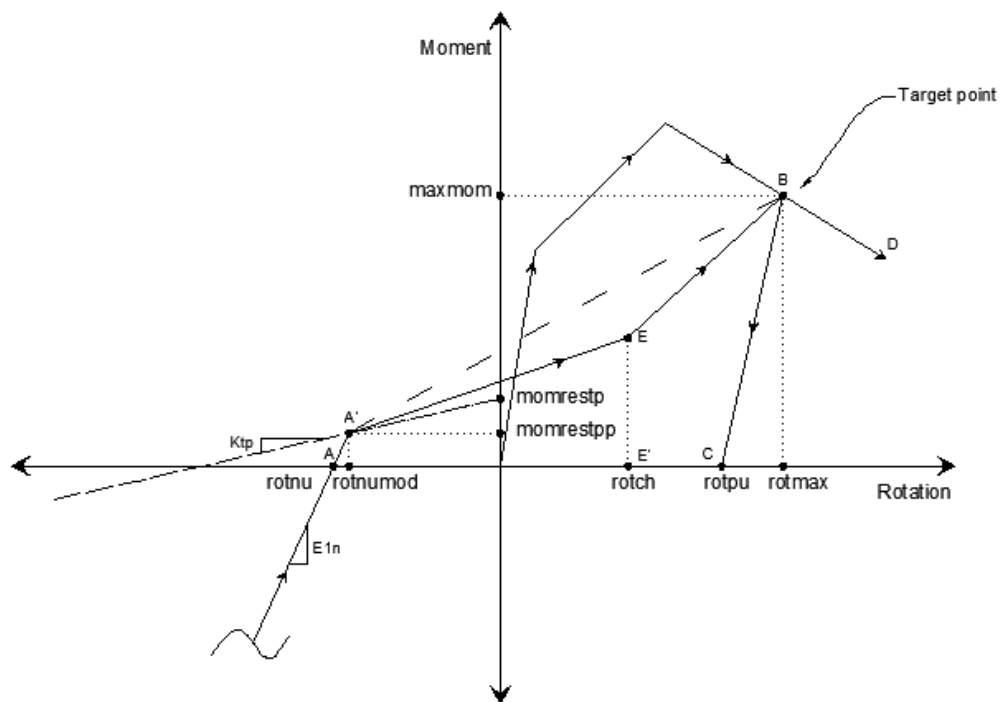


Figure 3.14: Decreasing residual moment behavior of the modified model

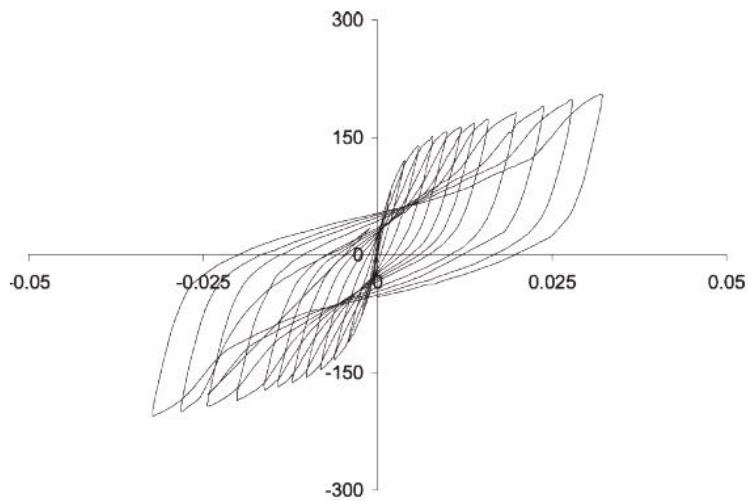


Figure 3.15: Experimental example of negative residual moment [3]

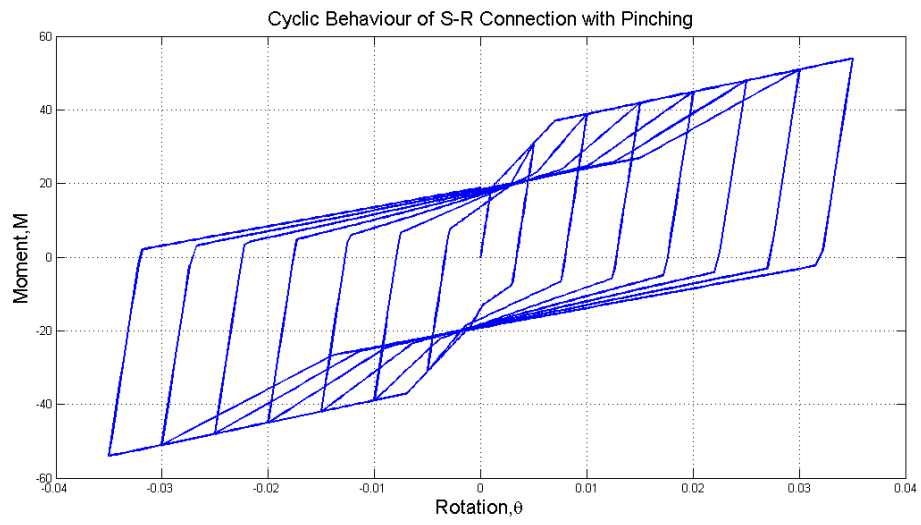


Figure 3.16 : A plot output of our modified model

CHAPTER 4

VERIFICATION

4.1 Verification of the semi-rigid mathematical model

The accuracy of the model presented in Section 3.4 can be validated with the test results of semi-rigid connections existing in the literature. The results obtained by Abolmaali, Kukreti and Razavi[3] were selected for this purpose. In their study two types of connections were tested namely bolted-bolted and welded-bolted double web angle connection. Bolted-bolted means angles are bolted to both beam web and column flange. Welded bolted means angles are welded to beam web and bolted to column flange. The configurations of these two connections are given in Appendix A. The connection between the angle and beam web is important. Because pinching mostly occurs due to enforcing of the bolts to the beam web. If the bolts have necessary strength, the circular bolt holes in the web will be oval shaped and if the angles have necessary strength the failure mode will be most probably web bearing. On the other hand when angles are welded to the beam web, due to high strength of weld, angle yielding governs the failure mode. In this study 5 bolted-bolted and 5 welded-bolted connections were used for validation. The results are shown in Figure 4.1 to Figure 4.10. In these figures DW-BB means bolted-bolted double web angle and DW-WB means welded-bolted double web angle. The numbers following these abbreviations are angle length, angle thickness, bolt diameter, column gauge, number of bolt rows, and beam depth respectively. The dimensions of beams and columns used for both connections (bolted-bolted and welded-bolted) were W410x67 and W200x100, respectively.

The test set up and loading history are given in Appendix A. As stated in the literature survey part of this thesis, load control mechanism is used to apply load up to a level. Once the rotation values at positive and negative peak moments starts to differ from each other due to plastic deformation, displacement control is applied until failure occurs in the experiments. Since the model presented in this study runs as a function of displacement, displacement control is used obligatorily in the program. The displacement history is different for each test. In the following 5 figures current model is compared with bolted-bolted double web angle (DW-BB) connections.

As it was stated earlier in bolted-bolted connections pinching takes place due to changing shape of the bolt holes from circle to ellipse. This effect can be seen in Figures 4.1, 4.3, 4.4, 4.5, clearly. On the other hand in Figure 4.2 pinching is less visible compared to others. This is due to reduced angle thickness in this specimen; thus angle yields before the initiation of pinching. This variation in the real behavior is not a big issue for the proposed model. By adjusting the pinching parameters, the proposed model can successfully simulate the behavior with an acceptable accuracy.

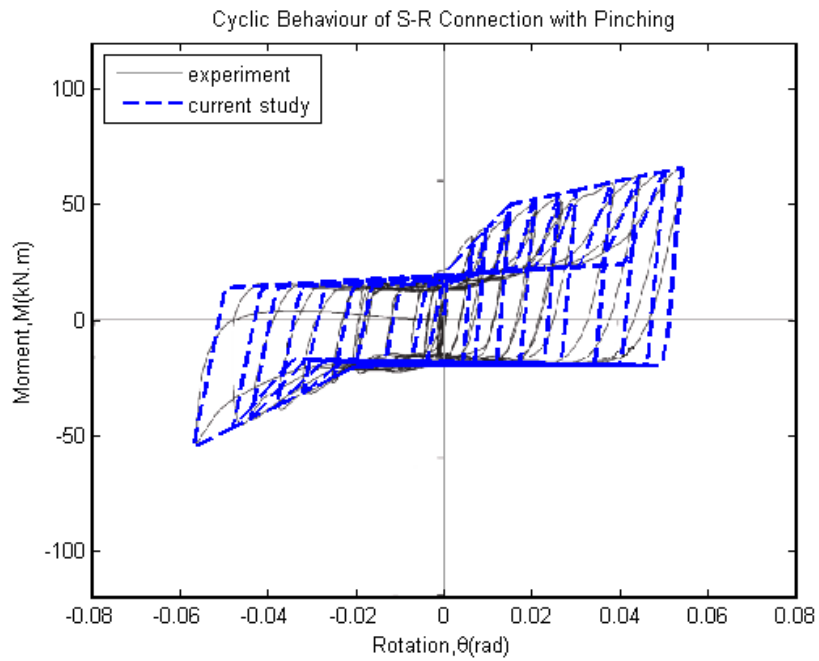


Figure 4.1: DW-BB-102-16-19-114-4-406

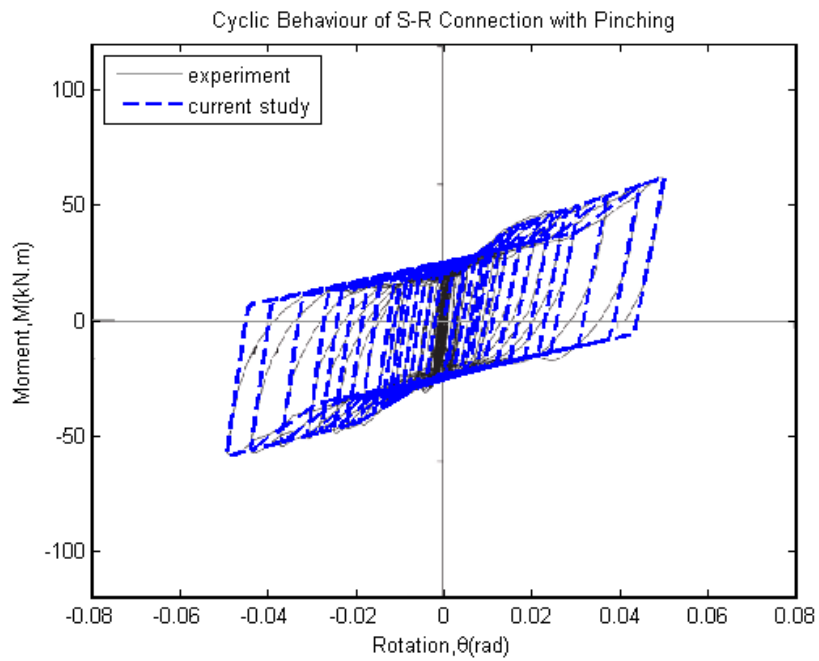


Figure 4.2: DW-BB-102-10-19-114-5-533

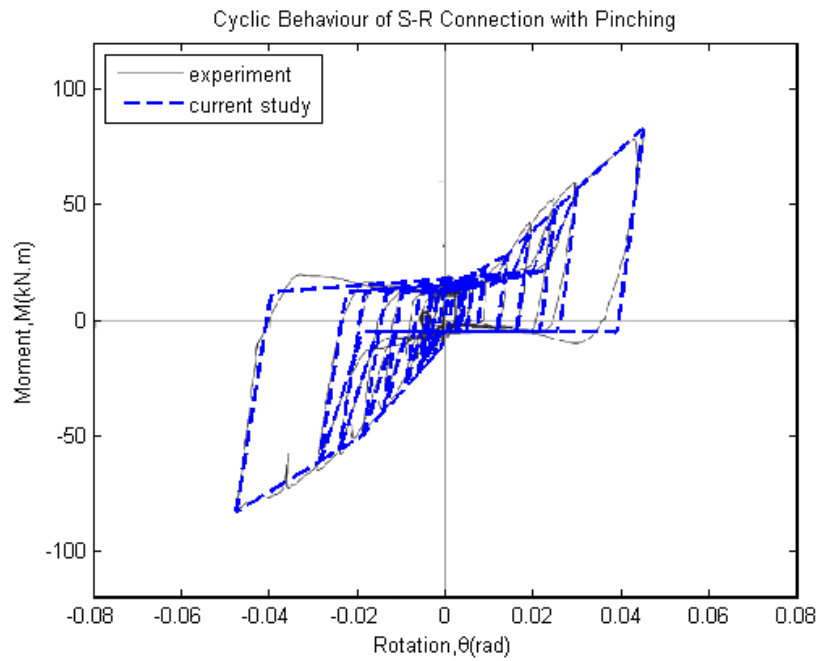


Figure 4.3: DW-BB-127-13-16-114-5-610

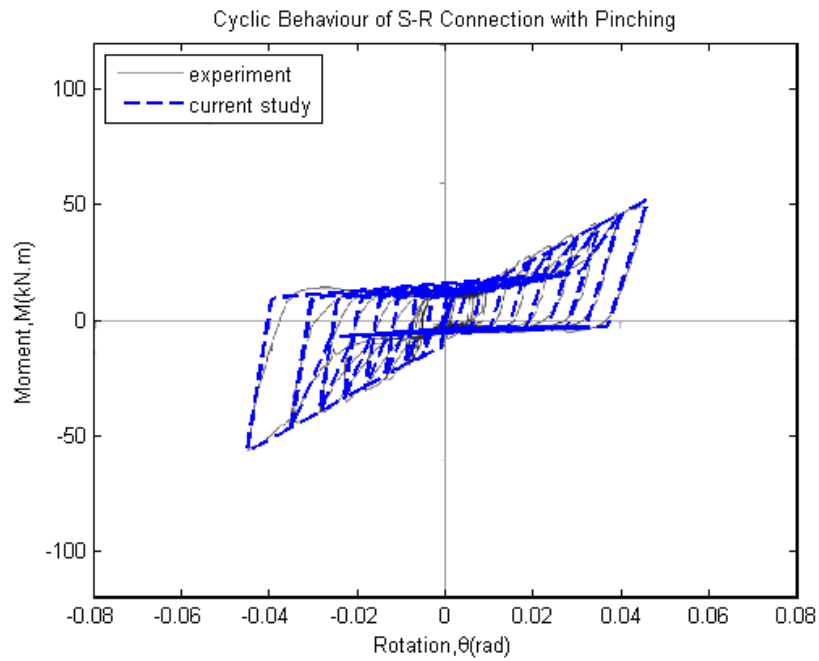


Figure 4.4: DW-BB-102-13-19-114-4-610

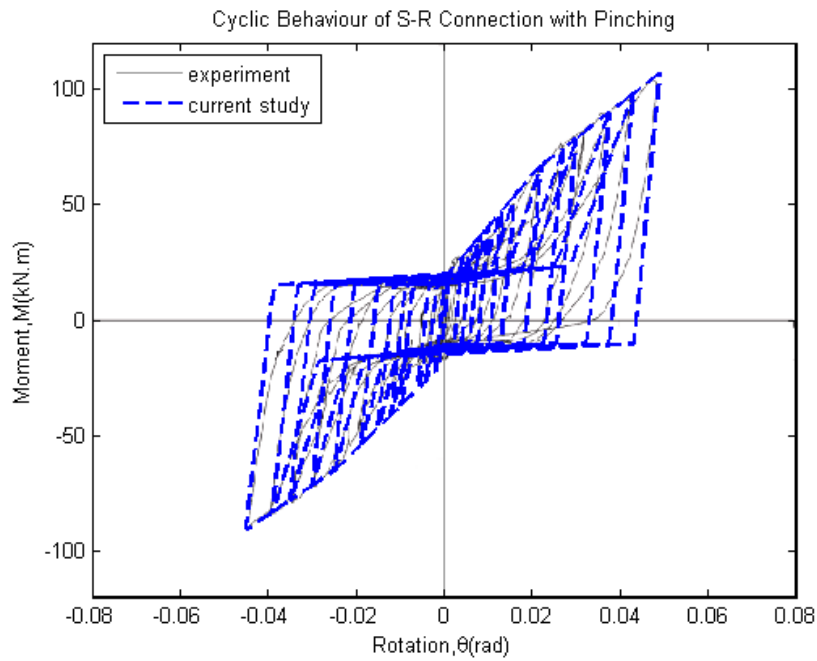


Figure 4.5: DW-BB-127-10-16-114-6-610

In the Figures 4.6-4.10 the results are presented for welded-bolted double web angle connections with varying geometric properties. It can be noted that since the angles are welded to the beam web, pinching occurs less relative to bolted-bolted double web angle connections. However in some cases for example the one shown in Figure 4.6 pinching is not negligible. This shows that other geometric properties such as column gauge also play a role in pinching.

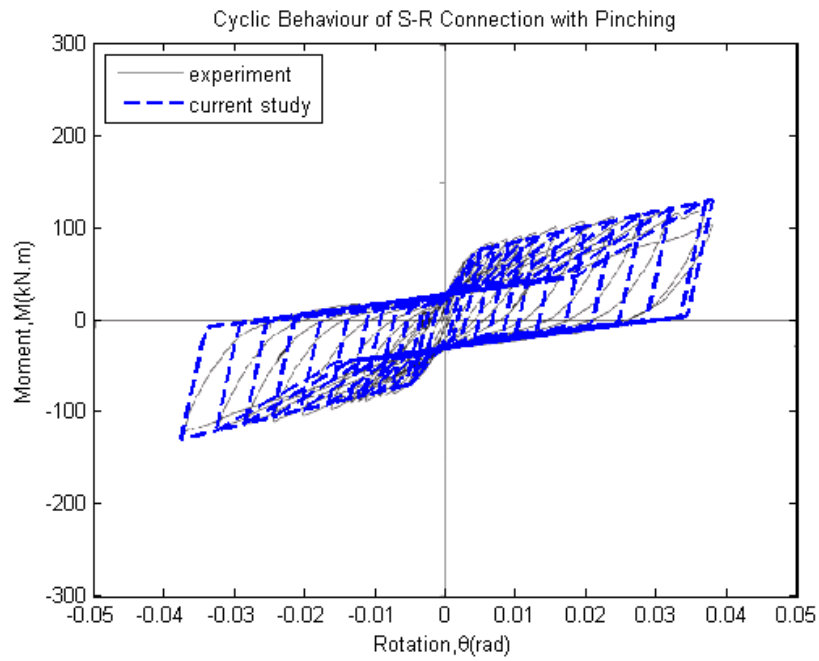


Figure 4.6: DW-WB-76-13-19-89-4-610

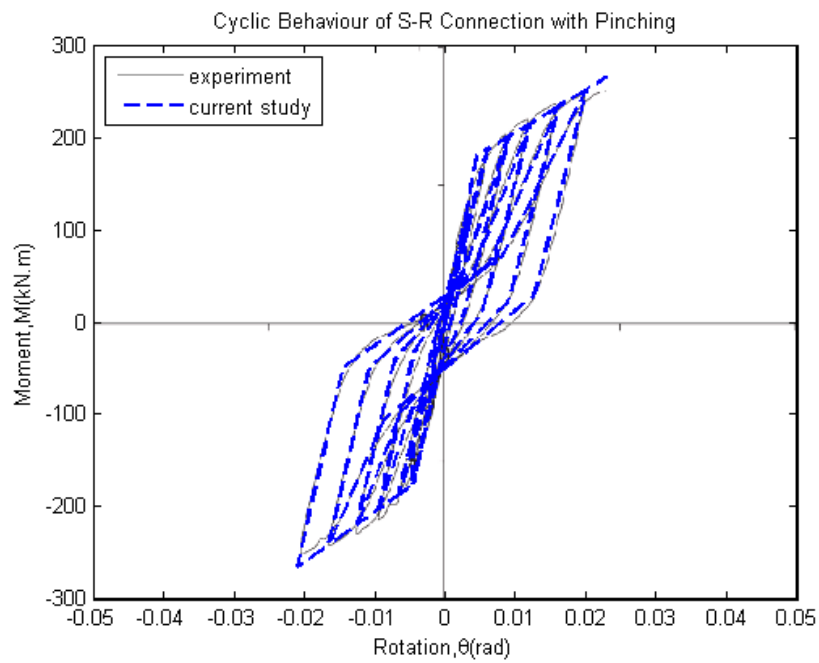


Figure 4.7: DW-WB-102-16-19-89-5-610

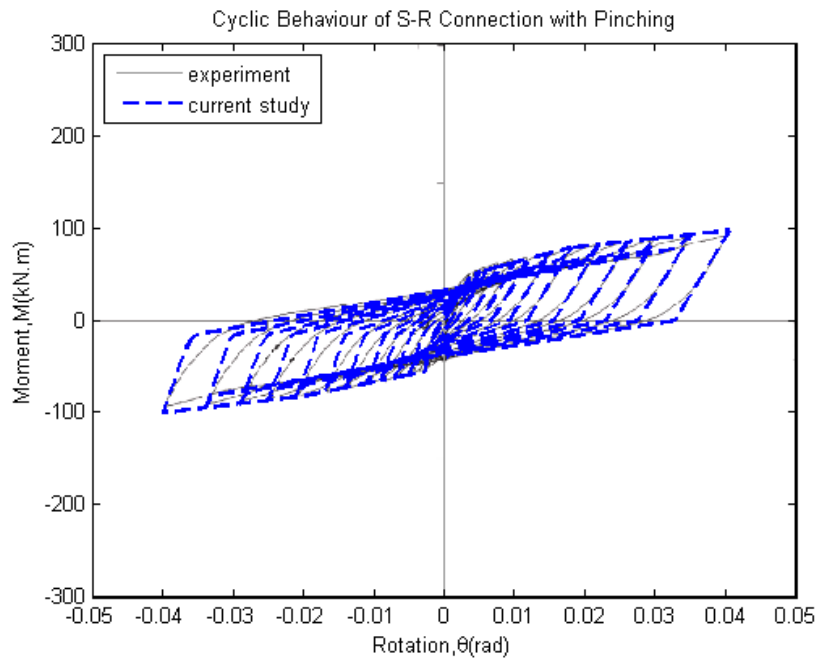


Figure 4.8: DW-WB-102-10-19-89-4-610

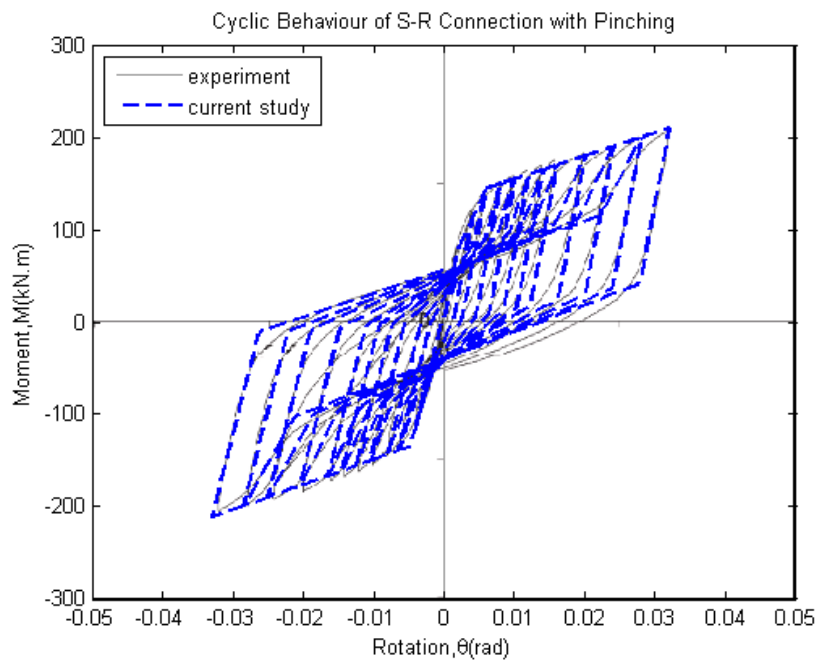


Figure 4.9: DW-WB-127-13-16-114-6-610

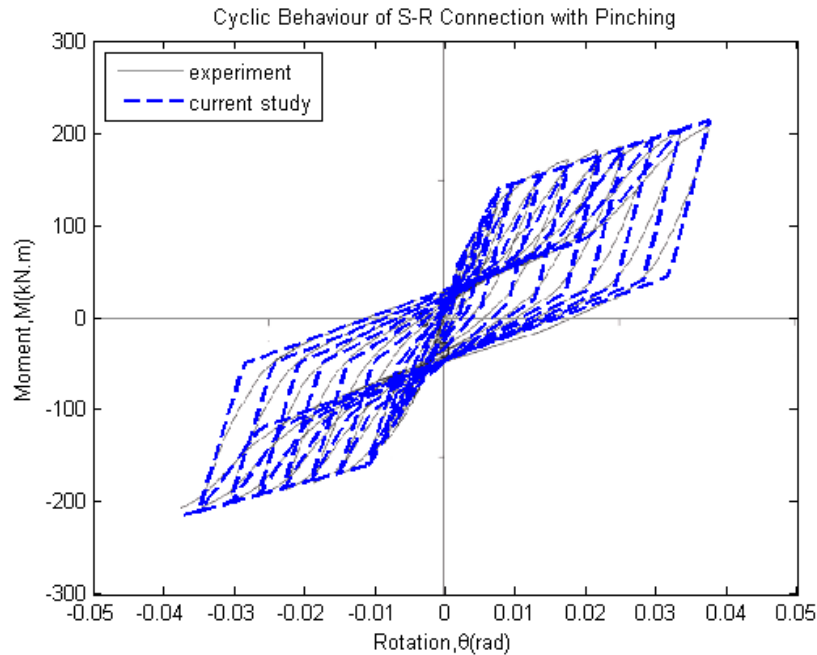


Figure 4.10: DW-WB-152-19-19-191-5-610

As a result it can be said that the proposed semi-rigid connection model presented in this thesis gives very accurate results with respect to given experimental tests. The parameters used for the proposed model are given in Appendix B, and these are selected from a large pool of parameters with the intent of matching the energy dissipation characteristics of the connection as close as possible. Calibration of the parameters at least requires an estimate of the initial stiffness, yield and plastic moment values of the connection, which can be obtained from various studies conducted on semi-rigid connectors. Calibration of the rest of the parameters on the other hand is a difficult task, and requires significant amount of experimental data and regression analysis.

4.2 Verification of the proposed element

In order to verify the response of the proposed macro element including semi-rigid connectors and to see the effect of the semi-rigid beam to column connections on the cyclic behavior of structures, a 3 story 1 bay structure is considered. All columns have 3.6 m length and IPE 330 section and all beams have 6 m length and IPE 300 sections; thus, ensuring strong column – weak beam design criteria. For all columns and beams bi-linear hysteretic steel material with following properties is used along element length, where each element is monitored at 5 Lobatto integration points, and at each section 4 and 8 layers are used in each flange and web, respectively;

$$f_y = 355 \text{ MPa}, E = 200 \text{ GPa and } E_h = 0.01 * E$$

For semi-rigid connections of beams the parameters used in a welded-bolted connection (DW-WB-152-19-19-191-5-610) presented in the paper of Abolmaali, Kukreti and Razavi is considered, where that connection had pinching behavior in its cyclic response as shown in Figure 4.10 [3]. Initial

rotational stiffness of the selected connection is 30670 kN.m/rad; thus, the ratio between the initial stiffness of the connection with respect to the beam flexural rigidity of IPE300 section satisfies the partially restrained condition (See Eqn 4.1). In addition to this analysis case, an alternative analysis is also conducted, where bilinear response is present in the semi-rigid connection (See Figure 4.12) instead of the quadra-linear model with pinching. This comparison will demonstrate the effect of the pinching behavior on the energy absorption during cyclic loading.

$$2 < \alpha = R_{ki} \times (L/EI)_{\text{beam}} \cong 11 < 20$$

4.1

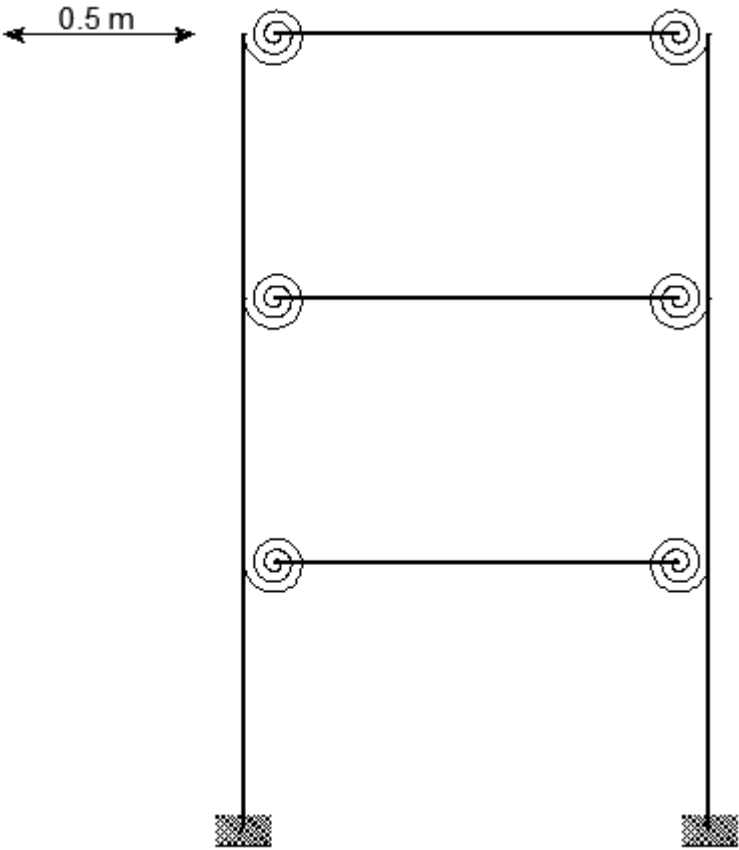


Figure 4.11: The 3 storey 1 bay structure model including semi-rigid connections

For the loading, a cyclic displacement reversal with a magnitude of 0.5 m is applied at the roof level. 4 different cases are examined to show the semi-rigid, nonlinear geometry and pinching effects;

Rigid connectors with linear geometry (LG-Rigid)

Rigid connectors with nonlinear geometry (NLG-Rigid)

Semi-Rigid connectors with linear geometry (LG-SR)

Semi-Rigid connectors with nonlinear geometry (NLG-SR)

Semi-Rigid connectors with linear geometry with bi-linear section model (LG-SR(Bi-Linear model))

Semi-Rigid connectors with nonlinear geometry with bi-linear section model (NLG-SR(Linear model))

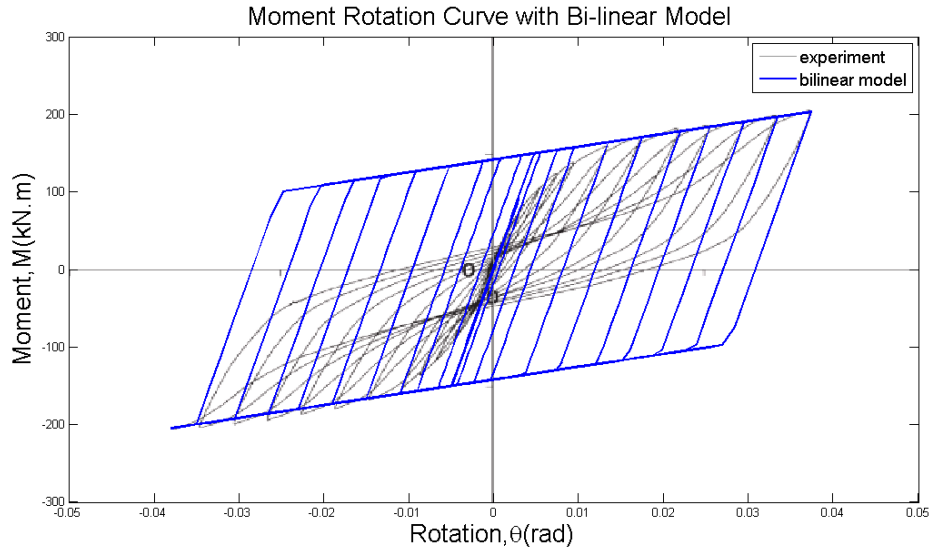


Figure 4.12: Bilinear model for selected connection, DW-WB-152-19-19-191-5-610.

In Figure 4.13, the responses obtained from the rigid and semi-rigid cases clearly demonstrate the importance of the linear and nonlinear behavior of semi-rigid connections. The difference in the energy absorption capacities between the bilinear model and quadra-linear model with pinching and damage for semi-rigid connections furthermore presents the necessity of development and use of advanced hysteretic models for the description of the nonlinear response of structures under earthquake excitations.

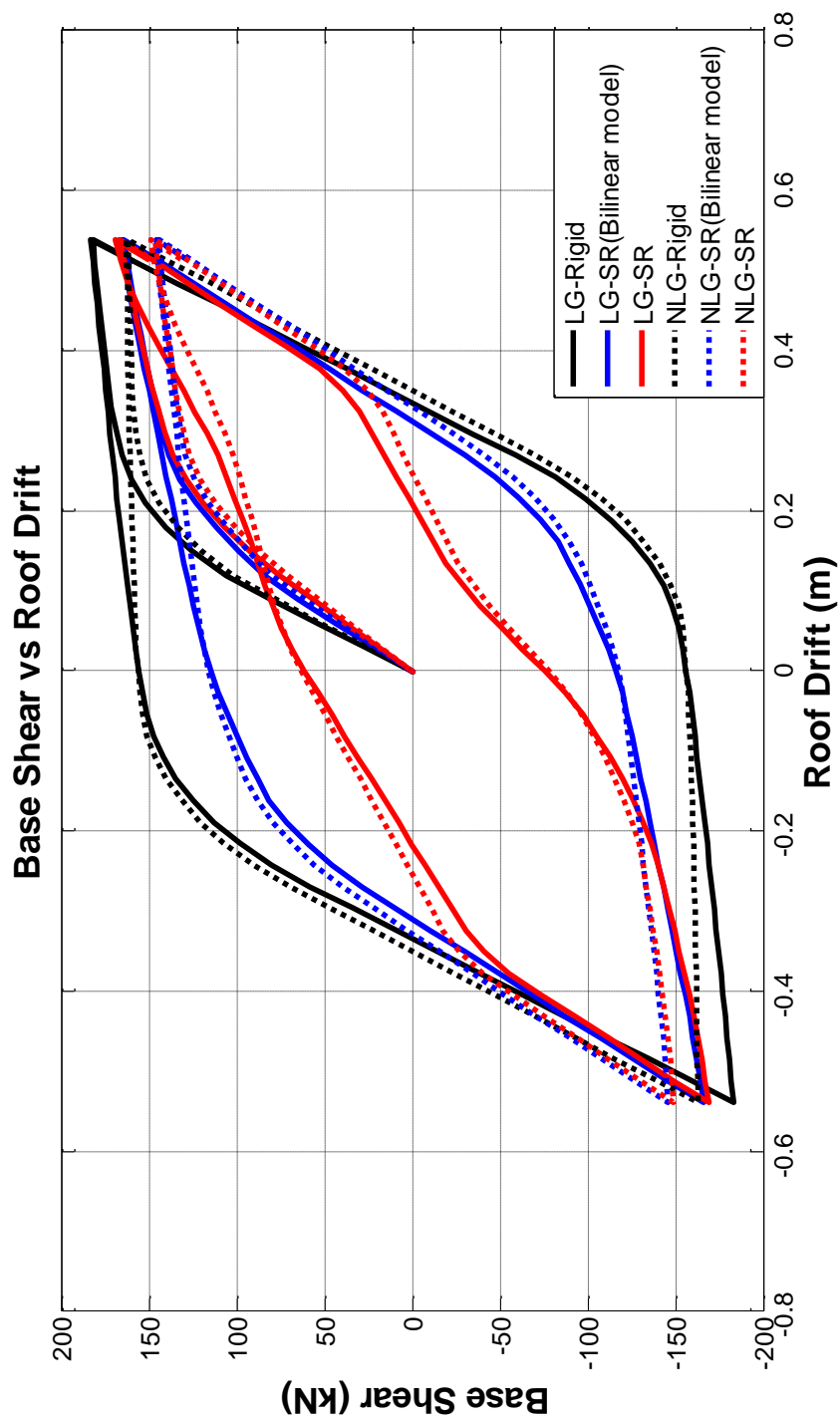


Figure 4.13: Effects of semi-rigid connection, pinching and nonlinear geometry on story drift

CHAPTER 5

SUMMARY, CONCLUSION AND RECOMMENDATIONS

5.1 Summary and Conclusion

The main purpose of this thesis is to incorporate the nonlinear and cyclic behaviors of the partially restrained steel connections into structural analyses. For this purpose, first, a macro frame element including connectors is developed. The formulation of the presented macro element is based on force formulation. As a second part of this thesis a hysteretic section model is developed. With this section model the cyclic behavior of semi-rigid connections is successfully simulated. Furthermore this model is calibrated via experimental data present in the literature. In addition to this, in order to verify the developed element and show the effects of semi-rigid connections, pinching and nonlinear geometry on the structural analyses, a 3 story building is analyzed with the developed beam element including semi-rigid connections. Based on this study following conclusions can be drawn:

- An accurate and robust beam element with semi-rigid connections is developed, where the element derivation bases on force formulation. With this element it is possible to incorporate semi-rigid connectors' behavior into analysis with less degree of freedom with respect to displacement based element.
- With this element it is also possible to capture the behavior of the spread of plasticity along element length in the beam span, as well. Also developed macro element can include any number of connectors located at anywhere along the beam; thus column tree connections can be easily analyzed by using single element per span by using the proposed beam element.
- A hysteretic section model is developed for capturing the cyclic behavior of semi-rigid connections. With some modifications such as pinching and residual moment behavior, moment rotation curves very close to experimental ones are obtained.
- The developed section model can easily be incorporated into the developed macro element. Thus a more realistic structural analysis can be performed with this element.
- Effect of semi-rigid connections on the initial lateral stiffness of the building is observed by comparing the rigid connection case. A lateral stiffness reduction is observed due to semi-rigid behavior of the connections.
- Effect of pinching on the energy absorption of the building is observed by comparing the results with the bilinear modeling approach of the semi-rigid connection, i.e. pinching in the connection is ignored with this analysis case. It is seen that pinching of the connections reduces the energy absorption of the building significantly, and should be incorporated into the modeling when earthquake excitations will be considered through a static cyclic or nonlinear time history analyses.
- Effect of nonlinear geometry is observed in the structural system response, and it is seen that for each case nonlinear geometry effect leads to softening in the building.

5.2 Future research recommendations

Several structural analyses can be performed to observe the effect of the semi-rigid connection behavior to the structure response such as story drift and natural frequency. The presented beam

element is formulated in 2D, so a 3D version of this element can be developed. The hysteretic section model is also developed in 2D and it can be modified to 3D, as well. The parameters used to capture the experimental behavior of the semi-rigid behavior in this thesis can be based on a broad range of connection topology through further study of different connection types. Finally, analysis of the structures that includes column tree members in which beam to column connections are located over the beam instead of column face can be performed with this element.

REFERENCES

1. Daz, C., et al., *Review on the modelling of joint behaviour in steel frames*. Journal of Constructional Steel Research, 2011. **67**(5): p. 741-758.
2. Popov, E.P. and S.M. Takhirov, *Bolted large seismic steel beam-to-column connections part 1: Experimental study*. Engineering Structures, 2002. **24**(12): p. 1523-1534.
3. Abolmaali, A., A.R. Kukreti, and H. Razavi, *Hysteresis behavior of semi-rigid double web angle steel connections*. Journal of Constructional Steel Research, 2003. **59**(8): p. 1057-1082.
4. Frye, M.J. and G.A. Morris, *ANALYSIS OF FLEXIBILITY CONNECTED STEEL FRAMES*. Canadian Journal of Civil Engineering, 1975. **2**(3): p. 280-291.
5. Kukreti, A.R., T.M. Murray, and A. Abolmaali, *End-plate connection moment-rotation relationship*. Journal of Constructional Steel Research, 1987. **8**(C): p. 137-157.
6. Krishnamurthy, N., et al., *Analytical $M-\phi$ curves for end-plate connections*. Journal of the Structural Division 1979. **45**: p. 105-133.
7. Kishi, N., et al., *Analysis program for the design of flexibly jointed frames*. Computers and Structures, 1993. **49**(4): p. 705-713.
8. Yee, Y.L. and R.E. Melchers, *MOMENT-ROTATION CURVES FOR BOLTED CONNECTIONS*. Journal of structural engineering New York, N.Y., 1986. **112**(3): p. 615-635.
9. Bahaari, M.R. and A.N. Sherbourne, *3D simulation of bolted connections to unstiffened columns-II. Extended endplate connections*. Journal of Constructional Steel Research, 1996. **40**(3): p. 189-223.
10. Chasten, C.P., L.-W. Lu, and G.C. Driscoll, *Prying and shear in end-plate connection design*. Journal of structural engineering New York, N.Y., 1992. **118**(5): p. 1295-1311.
11. Gebbeken, N., H. Rothert, and B. Binder, *On the numerical analysis of endplate connections*. Journal of Constructional Steel Research, 1994. **30**(2): p. 177-196.
12. Krishnamurthy, N. and D.E. Graddy, *Correlation between 2- and 3-dimensional finite element analysis of steel bolted end-plate connections*. Computers and Structures, 1976. **6**(4-5): p. 381-389.
13. Kukreti, A.R., T.M. Murray, and M. Ghassemieh, *Finite element modeling of large capacity stiffened steel tee-hanger connections*. Computers and Structures, 1989. **32**(2): p. 409-422.
14. Citipitioglu, A.M., R.M. Haj-Ali, and D.W. White, *Refined 3D finite element modeling of partially-restrained connections including slip*. Journal of Constructional Steel Research, 2002. **58**(5-8): p. 995-1013.
15. Castellazzi, G., *Analysis of second-order shear-deformable beams with semi-rigid connections*. Journal of Constructional Steel Research, 2012. **79**: p. 183-194.
16. Lui, E.M. and W.F. Chen, *Analysis and behaviour of flexibly-jointed frames*. Engineering Structures, 1986. **8**(2): p. 107-118.
17. Sekulovic, M. and R. Salatic, *Nonlinear analysis of frames with flexible connections*. Computers and Structures, 2001. **79**(11): p. 1097-1107.
18. Sekulovic, M., R. Salatic, and M. Nefovska, *Dynamic analysis of steel frames with flexible connections*. Computers and Structures, 2002. **80**(11): p. 935-955.
19. Valipour, H.R. and M. Bradford, *An efficient compound-element for potential progressive collapse analysis of steel frames with semi-rigid connections*. Finite Elements in Analysis and Design, 2012. **60**: p. 35-48.

20. Kishi, N., et al., *Design aid of semi-rigid connections for frame analysis*. Engineering Journal, 1993. **30**(3): p. 90-107.
21. Castellazzi, G., *Analysis of second-order shear-deformable beams with semi-rigid connections*. Journal of Constructional Steel Research, 2012. **79**(0): p. 183-194.
22. Valipour, H.R. and M. Bradford, *An efficient compound-element for potential progressive collapse analysis of steel frames with semi-rigid connections*. Finite Elements in Analysis and Design, 2012. **60**(0): p. 35-48.
23. Saritas, A. and O. Soydas, *Variational base and solution strategies for non-linear force-based beam finite elements*. International Journal of Non-Linear Mechanics, 2012. **47**(3): p. 54-64.
24. Taylor, R.L., et al., *A mixed finite element method for beam and frame problems*. Computational Mechanics, 2003. **31**(1-2 SPEC.): p. 192-203.
25. Ding, J. and Y.C. Wang, *Experimental study of structural fire behaviour of steel beam to concrete filled tubular column assemblies with different types of joints*. Engineering Structures, 2007. 29(12): p. 3485-3502.
26. Wilson WM, Moore HF. Tests to determine the rigidity of riveted joints in steel structures. In: University of Illinois. Engineering experiment station. Bulletin 104, Urbana (USA): University of Illinois; 1917.
27. Steel Structures Research Committee. Second report. London: Department of Scientific and Industrial Research, HMSO; 1934.
28. Faella C, Piluso V, Rizzano G. Structural steel semirigid connections: theory, design and software. In: New directions in civil engineering. Boca Raton (FL(EEUU)): CRC Publishers; 2000.
29. Suarez LE, Singh MP, Matheu EE. Seismic response of structural frameworks with flexible connections. Comput Struct 1996;58:27-41.
30. Aboutaha, R.S., "Seismic Shear Strengthening of R/C Columns Using Rectangular Steel Jackets", Ph.D. Dissertation, University of Texas at Austin, December 1994.

APPENDIX A

STANDARDIZATION PARAMETERS AND CURVE-FITTING CONSTANT FOR FRYE-MORRIS MODEL

**Table A.1: Standardization parameters and curve-fitting constants for Frye and Morris power model
(all size are in centimeters)**

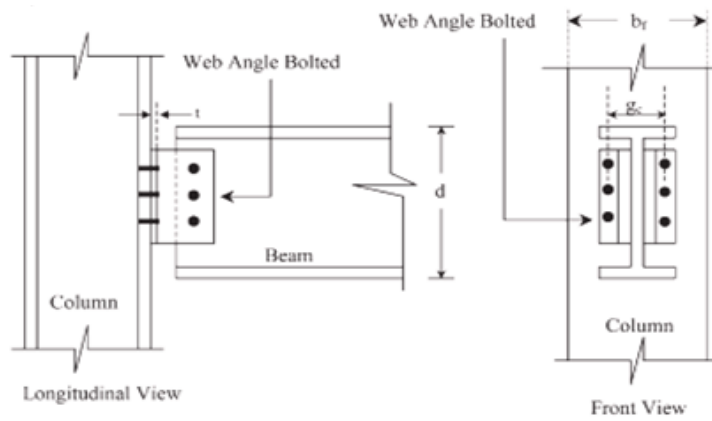
Connection Types	Curve-fitting constants	Standardization parameters
Single web-angle connection	$C_1 = 1.67 * 10^{-0}$ $C_2 = 8.56 * 10^{-2}$ $C_3 = 1.35 * 10^{-3}$	$K = d_a^{-2.4} * t_a^{-1.81} * g^{0.15}$
Double web-angle connection	$C_1 = 1.43 * 10^{-1}$ $C_2 = 6.79 * 10^1$ $C_3 = 4.09 * 10^5$	$K = d_a^{-2.4} * t_a^{-1.81} * g^{0.15}$
Top- and seat-angle With double web angle connection	$C_1 = 1.50 * 10^{-3}$ $C_2 = 5.60 * 10^{-3}$ $C_3 = 4.35 * 10^{-3}$	$K = d^{-1.287} * t^{-1.128} * t_c^{-0.415} * I_a^{-0.694} * (g - \frac{d_b}{2})^{1.350}$
Top- and seat-angle connection	$C_1 = 2.59 * 10^{-1}$ $C_2 = 2.88 * 10^3$ $C_3 = 3.31 * 10^4$	$K = d^{-1.5} * t^{-0.5} * I_a^{-0.7} * d_b^{-1.1}$
Extended end-plate connection without column stiffeners	$C_1 = 8.91 * 10^{-1}$ $C_2 = -1.20 * 10^4$ $C_3 = 1.75 * 10^8$	$K = d_g^{-2.4} * t_p^{-0.4} * d_b^{-1.5}$
Extended end-plate connection with column stiffeners	$C_1 = 2.60 * 10^{-1}$ $C_2 = 5.36 * 10^2$ $C_3 = 1.31 * 10^7$	$K = d_g^{-2.4} * t_p^{-0.6}$
Header plate connection	$C_1 = 6.14 * 10^{-3}$ $C_2 = 1.08 * 10^{-3}$ $C_3 = 6.05 * 10^{-3}$	$K = t_p^{-1.6} * g^{1.6} * d_p^{-2.3} * t_w^{-0.5}$
T-stub connection	$C_1 = 6.42 * 10^{-2}$ $C_2 = 1.77 * 10^2$ $C_3 = -2.03 * 10^4$	$K = d^{-1.5} * t^{-0.5} * I_t^{-0.7} * d_b^{-1.1}$

APPENDIX B

STUDY OF ABOLMAALI, KUKRETI AND RAZAVI

B.1 Connection configurations, test setup and loading history

(a)



(b)

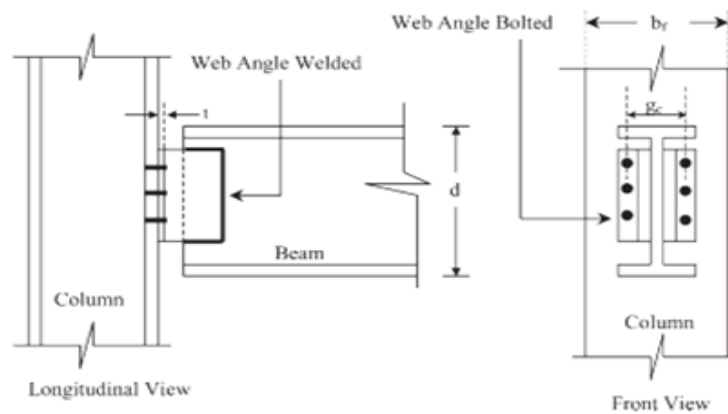


Figure B.1: Configuration of double web angle connections: (a) bolted-bolted; (b) welded-bolted.

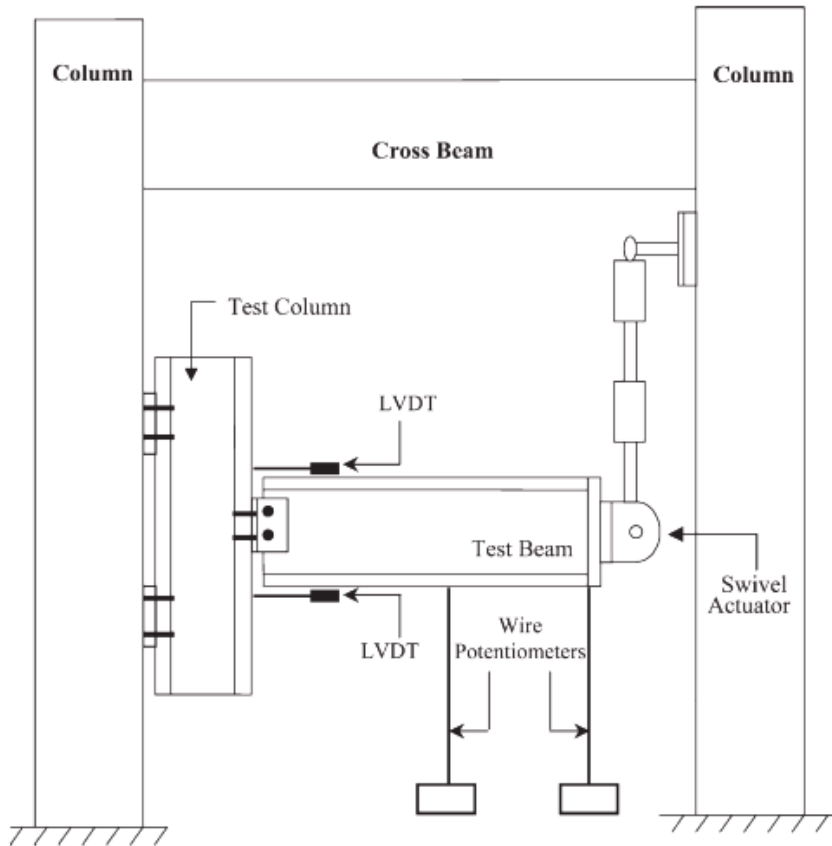


Figure B.2: Test setup and used instruments.

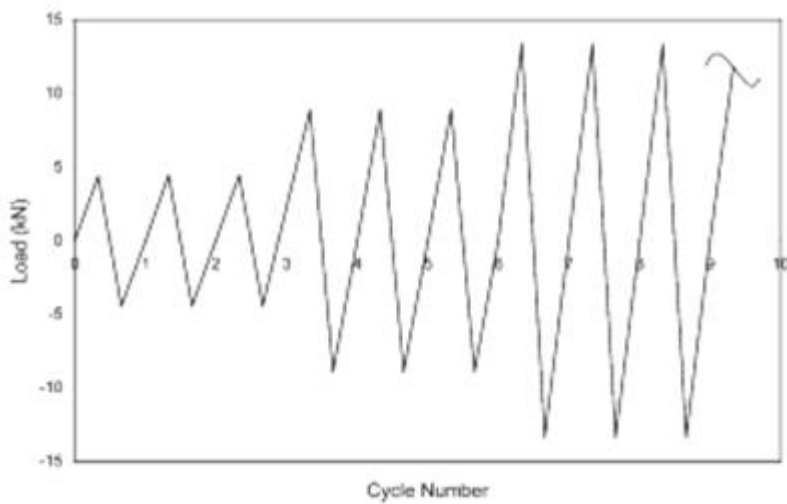


Figure B.3: Loading history

B.2 Geometric properties of bolted-bolted and welded connections

Table B.1: Geometric properties of the selected bolted-bolted connection

Test no. (1)	Test Designation DW-BB- l - t - b_d - g_c - N - d (2)	l (mm) (3)	t (mm) (4)	b_d (mm) (5)	g_c (mm) (6)	N (7)	d (mm) (8)
1	DW-BB-102-6- 19-114-3-406	102	6	19	114	3	406
2	DW-BB-102-6- 19-114-4-406	102	6	19	114	4	406
3	DW-BB-102-16- 19-114-4-406	102	16	19	114	4	406
4	DW-BB-102-6- 19-114-5-533	102	6	19	114	5	533
5	DW-BB-102-10- 19-114-5-533	102	10	19	114	5	533
6	DW-BB-102-10- 19-114-3-406	102	10	19	114	3	406
7	DW-BB-102-10- 19-114-4-406	102	10	19	114	4	406
8	DW-BB-127-13- 16-114-5-610	127	13	16	114	5	610
9	DW-BB-127-19- 19-114-5-610	127	19	19	114	5	610
10	DW-BB-102-13- 19-114-4-610	102	13	19	114	4	610
11	DW-BB-127-10- 16-114-4-610	127	10	16	114	4	610
12	DW-BB-127-10- 16-114-6-610	127	10	16	114	6	610

Table B.2: Geometric properties of the selected welded-bolted connections

Test no. (1)	Test designation DW-WB- l - t - b_d - g_c - N - d (2)	l (mm) (3)	t (mm) (4)	b_d (mm) (5)	g_c (mm) (6)	N (7)	d (mm) (8)
1	DW-WB-76-6-13-64-3-610	76	6	13	64	3	610
2	DW-WB-76-13-19-89-4-610	76	13	19	89	4	610
3	DW-WB-102-16-19-89-5-610	102	16	19	89	5	610
4	DW-WB-102-10-19-89-4-610	102	10	19	89	4	610
5	DW-WB-127-19-19-140-4-610	127	19	19	140	4	610
6	DW-WB-127-13-16-114-6-610	127	13	16	114	6	610
7	DW-WB-152-19-19-191-5-610	152	19	19	191	5	610
8	DW-WB-152-13-22-140-6-610	152	13	22	140	6	610

B.3 Test results

Table B.3: Test results and failure modes for selected bolted-bolted connections

Test no. (1)	Test designation DW-BB- <i>l-t-b_σg_c-N-d</i> (2)	Initial stiffness K_e ((kN m)/rad) (3)	Ultimate moment M_u (kN m) (4)	Ultimate rotation θ_u (rad) (5)	Failure mode (6)
1	DW-BB-102-6-19-114-3-406	1889	12	0.0500	Angle yielding
2	DW-BB-102-6-19-114-4-406	2966	21	0.0500	Angle yielding
3	DW-BB-102-16-19-114-4-406	18,649	63	0.0500	Web bearing
4	DW-BB-102-6-19-114-5-533	11,187	33	0.0500	Angle yielding
5	DW-BB-102-10-19-114-5-533	21,990	61	0.0500	Angle yielding
6	DW-BB-102-10-19-114-3-406	6074	19	0.0500	Angle yielding
7	DW-BB-102-10-19-114-4-406	13,812	39	0.0500	Angle yielding
8	DW-BB-127-13-16-114-5-610	19,268	80	0.0450	Web bearing
9	DW-BB-127-19-19-114-5-610	35,482	92	0.0450	Web bearing
10	DW-BB-102-13-19-114-4-610	12,204	50	0.0450	Web bearing
11	DW-BB-127-10-16-114-4-610	5690	37	0.0450	Yielding/bearing
12	DW-BB-127-10-16-114-6-610	17,854	93	0.0450	Angle yielding

Table B.3: Test results and failure modes for selected welded-bolted connections

Test no. (1)	Test designation DW-WB- <i>l-t-b_σg_c-N-d</i> (2)	Initial stiffness K_e ((kN m)/rad) (3)	Ultimate moment M_u (kN m) (4)	Ultimate rotation θ_u (rad) (5)	Failure mode (6)
1	DW-WB-76-6-13-64-3-610	5406	29	0.0315	Angle yielding/bolt fracture
2	DW-WB-76-13-19-89-4-610	28,538	120	0.0369	Angle yielding
3	DW-WB-102-16-19-89-5-610	54,699	253	0.0228	Bolt fracture
4	DW-WB-102-10-19-89-4-610	32,263	93	0.0395	Angle yielding
5	DW-WB-127-19-19-140-4-610	16,254	142	0.0395	Angle yielding
6	DW-WB-127-13-16-114-6-610	44,600	206	0.0320	Angle yielding
7	DW-WB-152-19-19-191-5-610	3067	204	0.0376	Angle yielding
8	DW-WB-152-13-22-140-6-610	45,443	202	0.0351	Angle yielding

APPENDIX C

PARAMETERS OF THE CURRENT MODEL

Table C.1: Parameters used in the current model (All moments are in kN.m and all rotations are in radian)

Model parameters	CONNECTION TOPOLOGIES									
	DW-BB-102-16-19-114-4-406	DW-BB-102-10-19-114-5-533	DW-BB-127-13-16-114-5-610	DW-BB-102-13-19-114-4-610	DW-BB-127-10-16-114-6-610	DW-WB-76-13-19-89-4-610	DW-WB-102-16-19-89-5-610	DW-WB-102-10-19-89-4-610	DW-WB-127-13-16-114-6-610	DW-WB-152-19-19-191-5-610
<i>mom1p</i>	22	20	15	12	20	35	30	50	80	60
<i>rot1p</i>	0,001	0,002	0,001	0,002	0,001	0,001	0,001	0,004	0,002	0,002
<i>mom2p</i>	50	40	28	20	65	75	180	78	145	140
<i>rot2p</i>	0,015	0,015	0,014	0,014	0,021	0,0045	0,0045	0,0178	0,006	0,0076
<i>mom3p</i>	66	62	83	52	107	130	265	97	210	215
<i>rot3p</i>	0,054	0,05	0,045	0,046	0,049	0,038	0,023	0,0405	0,032	0,038
<i>mom1n</i>	-19	-24	-12	-12	-20,5	-35	-50	-55	-60	-50
<i>rot1n</i>	-0,002	-0,0018	0,001	-0,001	0,0012	-0,001	-0,0015	-0,0026	-0,002	-0,002
<i>mom2n</i>	-20	-44,5	-50	-20	-65	-70	-175	-82	-135	-160
<i>rot2n</i>	-0,02	-0,02	-0,019	-0,01	-0,025	-0,005	-0,0045	-0,02	-0,005	-0,011
<i>mom3n</i>	-54	-59	-83	-57	-90	-130	-265	-100	-210	-220
<i>rot3n</i>	-0,056	-0,05	-0,0475	-0,045	-0,0445	-0,038	-0,021	-0,04	-0,0325	-0,04
<i>pinchxp</i>	0,9	0,62	0,9	0,9	0,85	0,6	0,6	0,95	0,8	0,63
<i>pinchyp</i>	0,2	0,6	0,2	0,3	0,1	0,4	0,4	0,87	0,6	0,54
<i>pinchxn</i>	0,9	0,6	0,9	0,9	0,9	0,6	0,65	0,95	0,8	0,75
<i>pinchyn</i>	-0,1	0,6	0	0,1	0,1	0,4	0,5	0,86	0,6	0,65
<i>momrestp</i>	15	20	12	10	15	15	-20	-15	0	-40
<i>momrestn</i>	-19	-23	-5	-3	-10	-20	0	0	0	5